

1 **Coupled Stratospheric Ozone and Atlantic Meridional Overturning**
2 **Circulation Feedbacks on the Northern Hemisphere Midlatitude Jet**
3 **Response to 4xCO₂**

4 Clara Orbe^{a,b}, David Rind^a, Darryn Waugh^c, Jeffrey Jonas^{a,d}, Xiyue Zhang^c, Gabriel Chiodo^e,
5 Larissa Nazarenko^{a,d}, and Gavin A. Schmidt^a

6 ^a *NASA Goddard Institute for Space Studies, New York, NY*

7 ^b *Department of Applied Physics and Applied Mathematics, Columbia University, New York, NY*

8 ^c *Department of Earth and Planetary Sciences, Johns Hopkins University, Baltimore, MD*

9 ^d *Center for Climate Systems Research, Earth Institute, Columbia University, New York, NY*

10 ^e *Institute for Atmospheric and Climate Science, ETH Zurich, Switzerland*

12 ABSTRACT: Stratospheric ozone, and its response to anthropogenic forcings, provide an im-
13 portant pathway for the coupling between atmospheric composition and climate. In addition to
14 stratospheric ozone's radiative impacts, recent studies have shown that changes in the ozone layer
15 due to $4\times\text{CO}_2$ have a considerable impact on the Northern Hemisphere (NH) tropospheric cir-
16 culation, inducing an equatorward shift of the North Atlantic jet during boreal winter. Using
17 simulations produced with the NASA Goddard Institute for Space Studies (GISS) high-top climate
18 model (E2.2) we show that this equatorward shift of the Atlantic jet can induce a more rapid weak-
19 ening of the Atlantic Meridional Overturning Circulation (AMOC). The weaker AMOC, in turn,
20 results in an eastward acceleration and poleward shift of the Atlantic and Pacific jets, respectively,
21 on longer timescales. As such, coupled feedbacks from both stratospheric ozone and the AMOC
22 result in a two-timescale response of the NH midlatitude jet to abrupt $4\times\text{CO}_2$ forcing: a "fast"
23 response (5-20 years) during which it shifts equatorward and a "total" response (~ 100 -150 years)
24 during which the jet accelerates and shifts poleward. The latter is driven by a weakening of the
25 AMOC that develops in response to weaker surface zonal winds, that result in reduced heat fluxes
26 out of the subpolar gyre and reduced North Atlantic Deep Water formation. Our results suggest
27 that stratospheric ozone changes in the lower stratosphere can have a surprisingly powerful effect
28 on the AMOC, independent of other aspects of climate change.

29 **1. Introduction**

30 There is large uncertainty in the atmospheric circulation response to increasing greenhouse gases
31 (see Shepherd (2014) and references therein). Although models generally predict a poleward shift
32 of the midlatitude eddy-driven jet, the magnitude of this shift is highly uncertain (e.g., Vallis et al.
33 (2015); Grise and Polvani (2014)) as are its underlying drivers (Shaw (2019)). This is especially
34 true in the Northern Hemisphere (NH), where there are opposing thermodynamic influences, i.e.
35 opposite meridional temperature gradient responses at the surface versus the upper troposphere
36 (Shaw et al. (2016)). Thus, while enhanced warming in the lower polar troposphere relative
37 to the lower tropical troposphere (i.e., Arctic amplification) contributes to reduced meridional
38 temperature gradients, increases in upper tropospheric tropical warming contribute to enhanced
39 temperature gradients aloft (Butler et al. (2010); Yuval and Kaspi (2020)) and it is not clear how
40 these competing processes affect the zonal mean midlatitude jet.

41 Many processes have been shown to influence the response of meridional temperature gradients
42 to increased CO₂, including polar amplification (see Smith et al. (2019) and references therein)
43 and cloud feedbacks (e.g., Ceppi and Hartmann (2015); Voigt and Shaw (2015)). By comparison,
44 composition feedbacks associated with the ozone response to CO₂ have been less well examined
45 although stratospheric ozone changes have been identified as an important pathway coupling
46 composition to climate (Isaksen et al. (2009)). In particular, the stratospheric ozone response to
47 4xCO₂ consists of robust decreases in the tropical lower stratosphere (LS), increases in the tropical
48 upper stratosphere and increases over high latitudes (Chiodo et al. (2018)). In the tropics, the
49 reductions in LS ozone are strongly correlated with the response of stratospheric upwelling (Fig.
50 6 in Chiodo et al. (2018)) and, while the exact details of these changes are model dependent,
51 especially over high latitudes, the general pattern is very consistent among models (e.g., Nowack
52 et al. (2015); Chiodo et al. (2018) and Chiodo and Polvani (2019) (hereafter CP2019)).

53 This pattern of reduced (increased) ozone over the tropical (high latitude) LS in response to
54 4xCO₂ has immediate implications for temperature gradients in the stratosphere by cooling the
55 tropics and warming high latitudes (Nowack et al. (2015); Chiodo et al. (2018); Li and Newman
56 (2022)). As CP2019 and Li and Newman (2022) showed, these changes in temperature gradients
57 drive an anomalous equatorward shift of the midlatitude jet in the Southern Hemisphere (SH).
58 In addition, both studies also showed shifts in the Northern Hemisphere (NH) during boreal

59 winter, where anomalies extend down into the lower troposphere and are concentrated over the
60 Atlantic, resembling the negative phase of the North Atlantic Oscillation (NAO). By comparison,
61 ozone feedbacks on LS temperature gradients do not result in a robust response of the Pacific jet
62 (CP2019).

63 A more recent study by Zhang et al. (2023) that considered two models – distinct from the ones
64 used in either CP2019 or Li and Newman (2022) – and that differed only in their representation
65 of interactive chemistry, also showed that changes in composition can impact the sign of the NH
66 midlatitude jet response to increased CO₂. However, in contrast to CP2019, the long-term impact
67 of this composition feedback was a *poleward*, not equatorward, shift of the zonal mean NH jet.
68 Though not investigated in detail, this poleward shift of the jet – expressed regionally as an eastward
69 extension of the Atlantic jet and a poleward shift of the Pacific jet – was linked to changes in the
70 ocean circulation, which were not examined in CP2019. More precisely, Zhang et al. (2023)
71 noted that the Atlantic Meridional Overturning Circulation (AMOC) exhibited a stronger decline
72 in interactive simulations in which trace gases and aerosols were allowed to respond to increased
73 CO₂, relative to non-interactive simulations. Indeed, recent studies have highlighted the large
74 influence that changes in the AMOC exert on the response of the NH midlatitude jet to increased
75 CO₂ (Gervais et al. (2019)), with models featuring a larger AMOC decline also tending to produce
76 a stronger and eastward extended jet over the Atlantic (Bellomo et al. (2021); Liu et al. (2020);
77 Orbe et al. (2023)).

78 The results from Zhang et al. (2023) suggest that composition feedbacks on the NH midlatitude
79 jet may depend on the response of the ocean circulation. However, that study did not examine
80 the mechanism underlying the stronger AMOC response in the interactive chemistry simulations
81 nor did it isolate the role of ozone from influences due to other trace gases and aerosols. To
82 this end, here we hypothesize that the ozone-induced negative NAO wind anomalies reported in
83 CP2019 provide a potential pathway through which stratospheric ozone changes can influence the
84 AMOC and the long-term response of the NH midlatitude jet. Our hypothesis is partly predicated
85 on results from previous studies showing that variations in the jet – namely those resembling the
86 NAO – can influence variability of the AMOC through changes in wind stress (Marshall et al.
87 (2001); Zhai et al. (2014); Delworth and Zeng (2016)). Modified air-sea fluxes of heat, water and
88 momentum associated with variations in the NAO alter vertical and horizontal density gradients in

89 the subpolar gyre, inducing changes in deep water formation and the AMOC (e.g., Visbeck et al.
90 (1998); Delworth and Dixon (2000)). This pathway via the NAO has been used to demonstrate how
91 sudden stratospheric warmings influence the variability of heat flux anomalies into the ocean and
92 ocean mixed layer depths in the North Atlantic (O’Callaghan et al. (2014)) as well as the strength
93 of the AMOC itself (Reichler et al. (2012)).

94 Here we present results from non-interactive and fully interactive chemistry global warming
95 experiments produced with the new high-top coupled atmosphere ocean version of the NASA
96 Goddard Institute for Space Studies (GISS) climate model that were submitted to the Coupled
97 Model Intercomparison Project Phase 6 (CMIP6) (Eyring et al. (2016)). We focus on simulations
98 in which CO₂ is abruptly doubled and quadrupled in order to facilitate comparison with the results
99 presented in CP2019 and Zhang et al. (2023).

100 We begin by verifying that reduced ozone in the tropical lower stratosphere, which is captured
101 only in the interactive simulations, leads to an equatorward shift of the midlatitude jet on relatively
102 fast timescales. Then we show that the AMOC response in the interactive simulations is largely
103 associated with these ozone-driven changes in the jet, not aerosols, using new experiments in
104 which the stratospheric ozone response to 4xCO₂ is isolated from changes in other trace gases and
105 aerosols. In particular, we show that our model captures the ozone-induced negative NAO-like
106 pattern first reported in CP2019; in addition, we also find that ozone-driven changes in surface
107 friction speed further weaken the AMOC, resulting in a long-term poleward shift of the NH jet.
108 As a result, we show that both stratospheric ozone changes and the AMOC influence the NH jet on
109 distinct “fast” and “total” timescales (and in the opposite sense), comprising a coupled atmosphere-
110 ocean feedback on the NH midlatitude jet response to increased CO₂. While the former “fast”
111 feedback was documented in CP2019, the latter has, to the best of our knowledge, not been reported
112 in previous studies.

113 We begin by discussing methods in Section 2 and then present key results and conclusions in
114 Sections 3 and 4, respectively.

115 2. Methods

116 *a. Model and Configurations*

117 Here we use the NASA Goddard Institute for Space Studies (GISS) “Middle Atmosphere (MA)”
118 Model E2.2 (Rind et al. (2020); Orbe et al. (2020)). E2.2 consists of 102 vertical levels spanning
119 the surface up to 0.002 hPa and is run at a horizontal resolution of 2 degrees by 2.5 degrees.
120 Orographic and non-orographic gravity wave drag is parameterized following Lindzen (1987)
121 and Rind et al. (1988), producing in E2.2 a quasibiennial oscillation (QBO) that compares well
122 with observations as well as improved stratospheric polar vortex variability (Ayarzagüena et al.
123 (2020); Rind et al. (2020)). Of most relevance to this study, Orbe et al. (2020) showed that E2.2
124 produces a significantly improved representation of the Brewer-Dobson and stratospheric transport
125 circulations, compared to the lower vertical resolution CMIP6 version of ModelE (E2.1, Kelley
126 et al. (2020)), resulting in reduced biases in ozone, methane, water vapor and nitrous oxide (see
127 their Figure 1). Among the different model versions discussed in Rind et al. (2020) and Orbe
128 et al. (2020) here we focus on the “Altered-Physics” (-AP) Version (E2.2-AP) because this is the
129 configuration that was submitted to CMIP6 and presented in recent studies (Ayarzagüena et al.
130 (2020); DallaSanta et al. (2021a,b)).

131 We begin by showing the results reported in Zhang et al. (2023) using both “Non-INTeractive”
132 (NINT) (Table 1, rows 1-3) and fully interactive “One-Moment Aerosols” (OMA) (Bauer et al.
133 (2020); Table 1, rows 4-6) configurations. In the NINT configuration all trace gases and aerosols
134 are set to preindustrial values. Hence, in the 2- and 4xCO₂ NINT runs neither ozone nor other trace
135 gases (besides water vapor) change in response to increased CO₂. By comparison, the OMA 2- and
136 4xCO₂ runs capture the full ozone response to CO₂, as well as composition feedbacks associated
137 with other trace gases and aerosols.

138 In order to isolate the role of ozone feedbacks on the circulation, we then perform experiments
139 using a linearized ozone (LINOZ) configuration (Table 1, rows 7-9). In LINOZ the stratospheric
140 ozone field is calculated interactively by Taylor expanding the equation of state around present-day
141 (2000–2010) values such that the ozone tendency is, to first-order, parameterized as a function of
142 the local ozone mixing ratio, temperature, and overhead column ozone (McLinden et al. (2000)).
143 Tropospheric ozone is calculated using monthly mean ozone production and loss rates archived

150 TABLE 1. The Model E2.2 experiments presented in this study, including preindustrial control, abrupt 2xCO₂
 151 and abrupt 4xCO₂ simulations using NINT (rows 1-3), OMA (rows 4-6) and LINOZ (rows 7-9) configurations.
 152 Four NINT abrupt 4xCO₂ ensemble members are included (row 3) in order to compare with a four member
 153 4xCO₂ ensemble produced using the LINOZ configuration (row 9). The 4xCO₂ ensemble mean LINOZ ozone
 154 response is also used to force four prescribed SST and SIC preindustrial experiments (row 10) in which all
 155 forcings other than ozone are set to preindustrial values. All coupled atmosphere-ocean simulations are run using
 156 the GISS Ocean v1 (GO1) (i.e., “-G” in CMIP6 notation).

Configuration	Ozone	CO ₂	Ensemble Size	SSTs and SICs
NINT	Preindustrial	Preindustrial	1	coupled (-G ocean)
NINT	Preindustrial	2xCO ₂	1	coupled (-G ocean)
NINT	Preindustrial	4xCO ₂	4	coupled (-G ocean)
OMA	Preindustrial	Preindustrial	1	coupled (-G ocean)
OMA	2xCO ₂	2xCO ₂	1	coupled (-G ocean)
OMA	4xCO ₂	4xCO ₂	1	coupled (-G ocean)
LINOZ	Preindustrial	Preindustrial	1	coupled (-G ocean)
LINOZ	2xCO ₂	2xCO ₂	1	coupled (-G ocean)
LINOZ	4xCO ₂	4xCO ₂	4	coupled (-G ocean)
NINT	LINOZ 4xCO ₂	Preindustrial	4	Prescribed Preindustrial

144 from GEOS-CHEM (Rind et al. (2014)). In contrast to NINT, therefore, the LINOZ ensemble
 145 captures the influence of the ozone response to CO₂ on the large-scale circulation. Unlike OMA,
 146 however, it is much more computationally efficient to run and isolates the ozone feedback from
 147 feedbacks related to other trace gases and aerosols. DallaSanta et al. (2021a) previously showed
 148 that the LINOZ ozone parameterization reproduces well the vertical structure and seasonal cycle
 149 of stratospheric ozone obtained from the fully interactive OMA configuration (see their Figure 1).

157 *b. Experiments*

158 For the different model configurations (NINT, OMA, LINOZ) we perform 150-year-long abrupt
 159 2- and 4xCO₂ experiments, in which CO₂ values are abruptly doubled and quadrupled relative to
 160 preindustrial concentrations. For each model configuration, these experiments are branched from
 161 a corresponding preindustrial control simulation. For NINT and LINOZ four-member 4xCO₂
 162 ensembles are run in order to assess the robustness of any ozone feedbacks. These experiments are
 163 all conducted using the atmosphere-ocean version of E2.2-AP that is coupled to the GISS Ocean

164 v1 (GO1) (i.e., “-G” in CMIP6 notation, hereafter simply E2.2-G). For coupled atmosphere-ocean
165 configurations in which (four-member) ensembles are run, different ensemble members are chosen
166 from different initial ocean states spaced 20 years apart in the corresponding preindustrial control
167 simulation.

168 In addition to the coupled atmosphere-ocean experiments, we also present results from a four-
169 member ensemble of 60-year-long atmosphere-only experiments in which sea surface temperatures
170 (SSTs) and sea ice concentrations (SICs) are fixed to preindustrial values, but the monthly mean
171 time-evolving ensemble mean ozone response from the coupled LINOZ 4xCO₂ experiments is
172 prescribed (Table 1, row 10). This allows us to quantify the impact of the ozone feedback
173 represented in LINOZ on the large-scale circulation, absent any contributions from changes in
174 background CO₂, sea ice concentrations or sea surface temperatures.

175 *c. Analysis*

176 1) TIMESCALES

177 When examining the midlatitude jet response to increased CO₂ we account for the fact that
178 extratropical circulation changes consist of distinct “fast” and “slow” responses (Ceppi et al. (2018),
179 hereafter CZS2018). More precisely, CZS2018 show that most of the shift of the midlatitude jets
180 occurs within 5-10 years of a steplike (abrupt) CO₂ forcing, with little shifts occurring during a
181 slower response over which SSTs change over subsequent decades. In contrast to the Southern
182 Hemisphere, zonal asymmetries play an important role in the Northern Hemisphere, where the
183 influence of local patterns in sea surface temperature change can result in oppositely signed jet
184 shifts between the Pacific and Atlantic ocean basins on “slow” timescales. Given this potential
185 for compensating jet shifts on distinct timescales, we therefore decompose the CO₂ circulation
186 response into “fast” and “total” timescale responses.

187 More precisely, we modify the original approach used in CZS2018 to define our “fast” response as
188 the difference between the ensemble mean 4xCO₂ response, averaged over years 5-20 (as opposed
189 to years 5-10), and the corresponding preindustrial control simulation. Calculations of the “fast”
190 response using years 5-10 produce similar results (not shown), but the choice of years 5-20 better
191 accounts for the large internal variability in our runs, perhaps related to a somewhat larger ENSO
192 amplitude in our model compared to observations (Rind et al. (2020)).

193 In addition, instead of focusing on the “slow” response, defined in CZS2018 as the difference
194 between averages over years 121-140 and years 5-10, here we examine the “total” response, defined
195 as the difference between the ensemble mean 4xCO₂ response, averaged over years 100-150, and the
196 preindustrial control simulation. This approach for defining the “total” response is not only more
197 consistent with what was used in Zhang et al. (2023) and CP2019, with which we directly compare
198 our results throughout, but also with numerous other studies examining the atmospheric circulation
199 response to an abrupt quadrupling of CO₂ (e.g., Grise and Polvani (2014, 2016); Menzel et al.
200 (2019)). Note that in response to an abrupt quadrupling of CO₂ the NINT model configuration
201 produces global mean surface temperature “fast” and “total” responses of ~2.9°C and ~3.9°C,
202 respectively.

203 Statistical significance of the four-member ensemble mean LINOZ-NINT and single member
204 OMA-NINT abrupt CO₂ differences is assessed using a two-sample Student’s t-test at the 95%
205 confidence level. Significance of differences is assessed relative to the interannual variability in
206 the corresponding preindustrial control simulation.

207 2) ANALYSIS FIELDS

208 In addition to the atmospheric variables examined in CP2019 (i.e., zonal mean wind, zonal mean
209 temperature, surface temperature, 850 hPa zonal wind) we examine ocean variables relevant to
210 understanding the evolution of the AMOC and its coupling to the atmosphere. In particular, in
211 addition to examining the surface mixed layer depths we also examine sea surface temperatures,
212 surface friction speed, horizontal ocean heat and salinity transports, as well as the net heat fluxes
213 which, together with the net freshwater fluxes (F; inferred from precipitation minus evaporation
214 (P-E)), provide information about the surface buoyancy forcing (Large and Yeager (2009)). In our
215 simulations, the preindustrial climatological buoyancy forcing over the North Atlantic is dominated
216 by the sum of the net heat fluxes ($Q = Q_H + Q_E + Q_S + Q_L$), which are defined to be positive into the
217 ocean (Appendix Figure A1, left). These are further partitioned into their respective latent heat
218 (Q_E) and sensible heat (Q_H) contributions, as we find that the net solar (Q_S) and longwave (Q_L)
219 flux radiative contributions are negligible over the North Atlantic region (Appendix Figure A1,
220 right).

221 Given our interest in the Northern Hemisphere and our expectations that stratospheric ozone feed-
222 backs on the NH jet will occur during boreal winter (CP2019), we focus primarily on December-
223 January-February (DJF). The ocean heat transport changes in our simulations are also most pro-
224 nounced during DJF, consistent with the analyses presented in Romanou et al. (2023) and Orbe
225 et al. (2023).

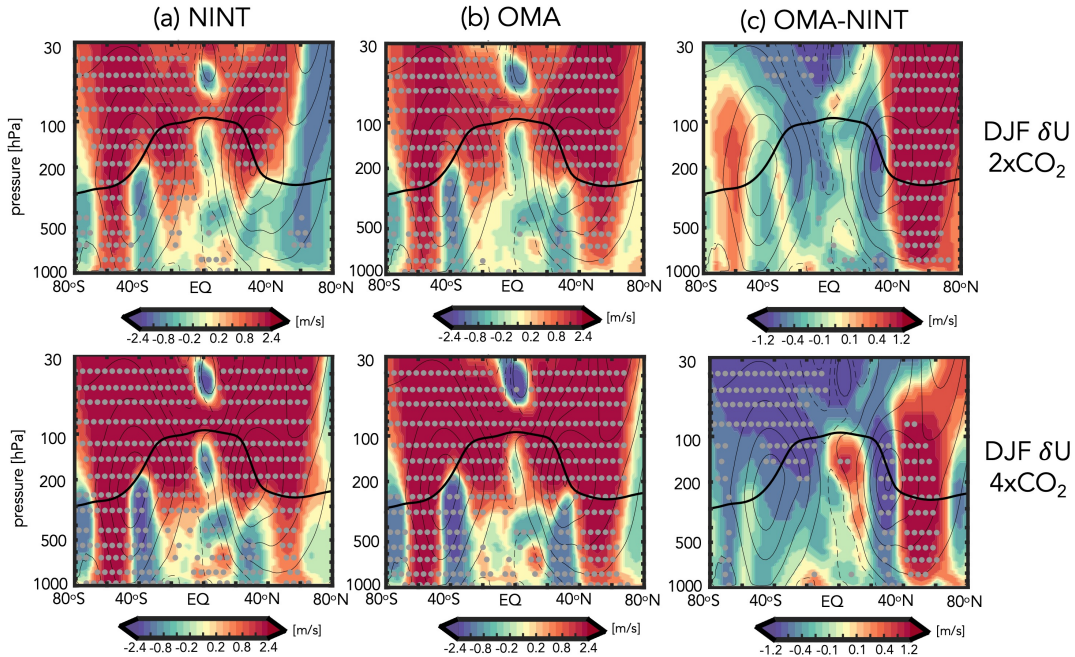
226 3. Results

227 *a. Abrupt 2xCO₂ and 4xCO₂ Zonal Mean Wind Response: OMA versus NINT*

228 Before focusing on ozone feedbacks, we first review the OMA versus NINT differences in NH
229 jet behavior that were presented in Zhang et al. (2023) (Figure 1). In the stratosphere the zonally
230 averaged DJF wind response to 2- and 4xCO₂ features an acceleration at nearly all latitudes,
231 consistent with amplified warming in the tropical upper troposphere (Shaw (2019)) and increased
232 cooling of the stratosphere with height (Garcia and Randel (2008)). Similar wind responses emerge
233 in both the NINT and OMA configurations, except over northern high latitudes at 2xCO₂, where
234 the zonal winds in NINT weaken and the response is not statistically significant.

243 In the troposphere, however, there are noticeable differences between the OMA and NINT
244 simulations. In particular, the NH midlatitude jet features a much stronger poleward shift in OMA,
245 compared to NINT (Figures 3 and 6 in Zhang et al. (2023)). As discussed in that study, the stronger
246 response in OMA results in enhanced eddy mixing along isentropes on the poleward flank of the
247 NH jet, resulting in increased transport of tracers from the northern midlatitude surface to the
248 Arctic (not shown). This difference between OMA and NINT occurs at both 2- and at 4xCO₂, such
249 that at 2xCO₂ the NH jet response is opposite in sign between NINT and OMA, while at 4xCO₂
250 the poleward jet shift is much stronger in OMA. In the SH, by comparison, the differences between
251 OMA and NINT are much smaller and not statistically significant.

252 Zhang et al. (2023) hypothesized that the different behaviors of the NH jet between the NINT
253 and OMA “total” responses were related to different responses in the behavior of the AMOC to
254 increased CO₂ forcing (Figure 2). That is, despite an initial weakening, the AMOC eventually
255 recovers to preindustrial values in the NINT 2xCO₂ simulation, in contrast to the total response
256 to 4xCO₂ in which the AMOC is about 10 SV weaker than the preindustrial control (Fig. 2, left,

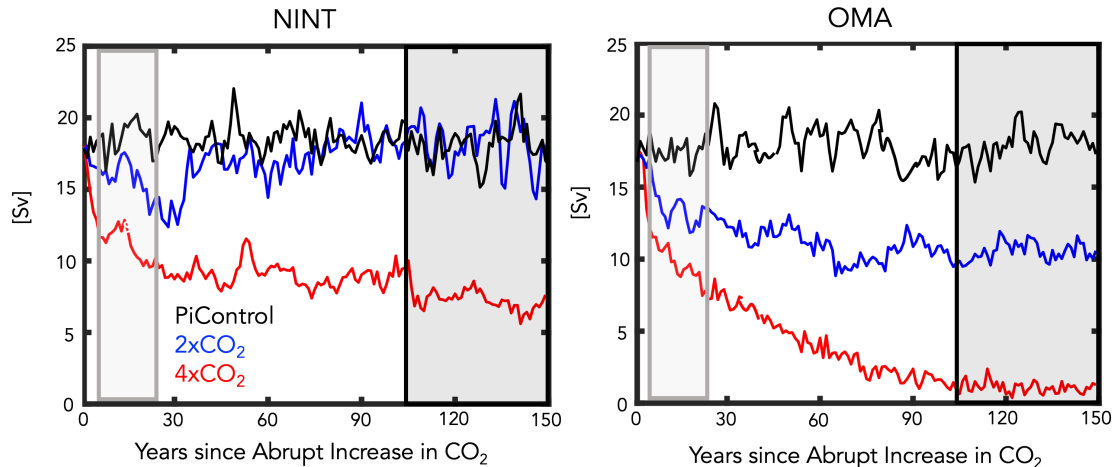


235 FIG. 1. Colors show the December-January-February (DJF) response of the zonal mean zonal winds, U , to
 236 an abrupt doubling (top) and quadrupling (bottom) of CO_2 , averaged over years 100-150. Results are shown
 237 for NINT (a,d) and fully interactive OMA configurations (b,e), where one ensemble member has been used for
 238 each forcing scenario. The OMA - NINT differences are also shown (c,f). Black contours denote climatological
 239 mean preindustrial control DJF U values (contour interval: 8 m/s). Stippled regions are statistically significant
 240 and the black thick line shows the climatological mean tropopause in the preindustrial control NINT simulation.
 241 Note that all colorbar bounds are consistent with those used in Chiodo and Polvani (2019) in order to facilitate
 242 comparisons with that study.

257 black box). By comparison, in the OMA configuration, the AMOC weakens significantly more,
 258 by ~ 7 SV and ~ 17 SV in the 2- and 4x CO_2 simulations, respectively (Fig. 2, right, black box).

263 As it is difficult to meaningfully interpret the zonal mean wind response in the NH, where there
 264 are large zonal variations in the midlatitude jet (Barnes and Polvani (2013); Simpson et al. (2014)),
 265 we next compare the 850 hPa zonal wind changes between the NINT and OMA 4x CO_2 simulations,
 266 further distinguishing between “fast” and “total” responses (Figure 3). We begin with the NINT
 267 equilibrated or “total” response (i.e. years 100-150), which consists of a poleward jet shift over the
 268 Pacific basin and an acceleration and eastward extension of the jet over the Atlantic and Eurasia
 269 (Fig. 3b). This pattern is amplified in the OMA run (Fig. 3d), in which both the strengthening

Annual Mean AMOC Response at 48°N



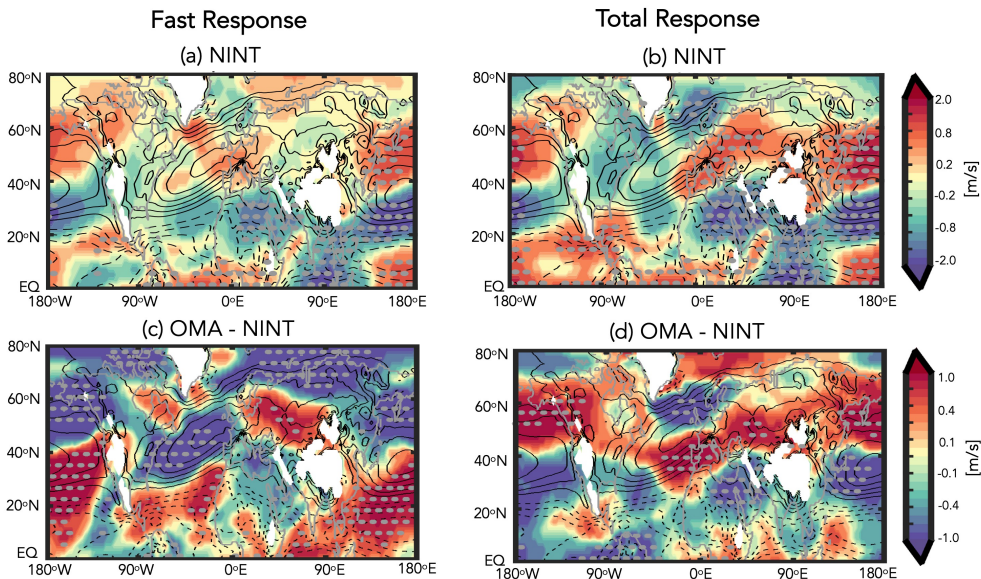
259 FIG. 2. Evolution of the annual mean maximum overturning stream function below 900 m in the Atlantic
 260 ocean, evaluated at 48°N, for the preindustrial control (black), abrupt 2xCO₂ (blue) and abrupt 4xCO₂ (red)
 261 simulations. Results for the NINT (left) and OMA (right) configurations are shown. Light grey and black shaded
 262 boxes denote the “fast” and “total” timescale response averaging periods.

270 and eastward extension of the jet over the Atlantic and its poleward shift over the Pacific are more
 271 pronounced. This amplified response in OMA over both the Pacific and Eurasia is also evident at
 272 300 hPa (Appendix Figure A2b).

273 This wind response in OMA, relative to NINT, is consistent with the jet differences identified
 274 in Orbe et al. (2023) between two non-interactive simulations of the GISS low-top climate model
 275 in which only the AMOC strength differed. The enhanced and eastwardly extension of the North
 276 Atlantic jet is also consistent with previous studies employing water hosing simulations (e.g.,
 277 Bellomo et al. (2023); Jackson et al. (2015)). This suggests that the jet differences between OMA
 278 and NINT on these longer timescales are primarily driven by differences in the AMOC response,
 279 as hypothesized in Zhang et al. (2023).

286 Figure 2 (grey boxes) highlights how the AMOC differences between OMA and NINT noted
 287 in Zhang et al. (2023) arise very early in the simulations (within the first 20 years). Over these
 288 years – which comprise the “fast” response – the impact of interactive chemistry on the zonal
 289 wind changes at 850 hPa is very different (Fig. 3a,c). In particular, over the Atlantic, interactive

DJF $4\times\text{CO}_2$ δU at 850 hPa



280 FIG. 3. Colors show the $4\times\text{CO}_2$ (four member) ensemble mean change in the DJF 850 hPa zonal winds
 281 for the NINT configuration, decomposed into “fast” (i.e. years 5-20) (a) and “total” (i.e. years 100-150) (b)
 282 responses. The OMA - NINT fast and total differences are shown in (c) and (d), respectively. Note that one
 283 ensemble member is used in displaying the OMA - NINT differences (same as used in Figure 1). Black contours
 284 denote climatological mean preindustrial control DJF values (U contour interval: 2 m/s) and stippled regions are
 285 statistically significant.

290 composition results in a strong weakening over the midlatitude jet core and an acceleration on the
 291 equatorward flank of the jet (Fig. 3c). This wind change is also evident at 300 hPa (not examined
 292 in CP2019), where the winds accelerate on the equatorward and poleward flanks of the midlatitude
 293 and subtropical jets, respectively (Fig. A2a). Over the Pacific, where the midlatitude jet is more
 294 vertically coherent, interactive chemistry results in an anomalous equatorward jet shift relative to
 295 the NINT simulation at both 850 hPa (Fig. 3a) and 300 hPa (Fig. A2a).

296 This fast composition feedback that occurs over years 5-20 is consistent with the results from
 297 CP2019, who showed that the ozone response to $4\times\text{CO}_2$ induces a weakening of the North Atlantic
 298 jet and a strengthening on its equatorward flank (see their Figure 6). This response is reminiscent
 299 of the negative phase of the NAO which previous studies have shown can result in a weaker
 300 AMOC (Delworth and Zeng (2016)). In CP2019, however, this response is realized through

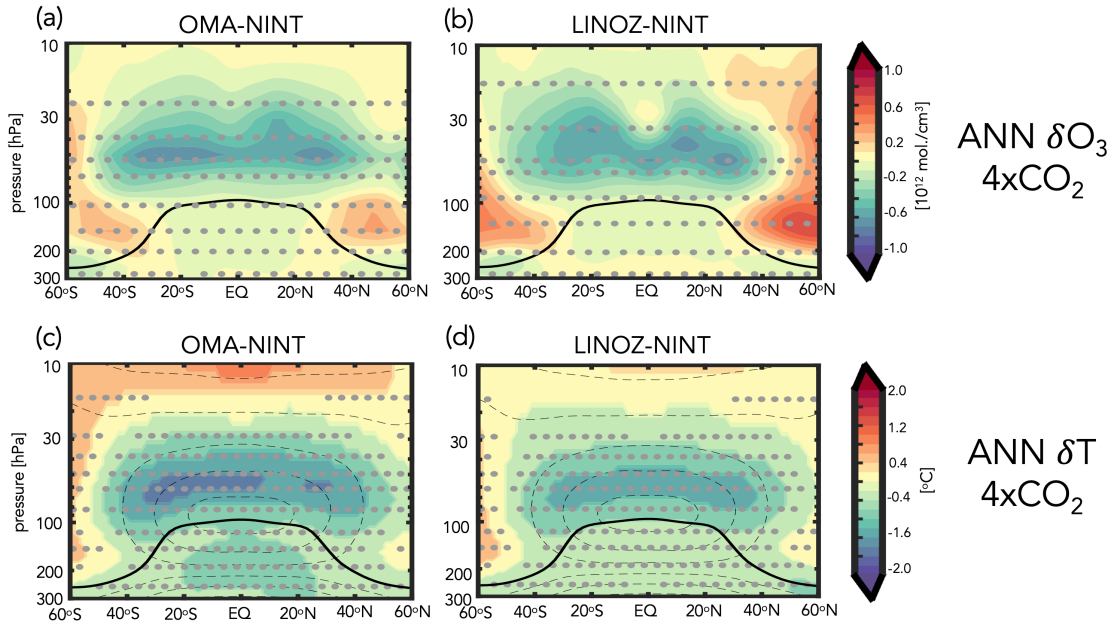
301 changes in stratospheric ozone alone, whereas in OMA all trace gases and aerosols are responding.
302 Furthermore, the significance of this rapid response with only one ensemble member is uncertain,
303 particularly during the first 5-20 years when the signal is confounded by large internal variability.
304 To this end, next we present results from the larger (4-member) LINOZ ensemble to examine
305 whether the fast response in the NH jet is related to stratospheric ozone changes.

306 *b. Abrupt 4xCO₂ Stratospheric Ozone and Temperature Responses: OMA versus LINOZ*

307 Before examining the circulation response in the LINOZ ensemble, we first compare the annually
308 averaged ensemble mean LINOZ 4xCO₂ ozone response with that from the OMA simulation (Figure
309 4). The amplitude and pattern of the ozone response in the LINOZ ensemble (Fig. 4b) is generally
310 very similar to the ozone response in the OMA simulation (Fig. 4a), consistent with Meraner et al.
311 (2020), who showed that the response of ozone to a quadrupling of CO₂ is well captured using
312 linearized ozone schemes. In both OMA and LINOZ configurations the pattern of the 4xCO₂
313 changes reflects a decrease in tropical LS ozone, associated with enhanced tropical upwelling
314 (Garcia and Randel (2008)), and enhanced concentrations over high latitudes. Over all latitudes
315 the ozone changes are statistically significant, relative to interannual variability in the preindustrial
316 control simulation.

324 Over northern high latitudes there are some differences in the mid-to-lower stratosphere (~30-100
325 hPa) between LINOZ and OMA, generally consistent with Chiodo et al. (2018), who found that
326 in this region the ozone response to CO₂ is more dependent on (nonlinear) chemical and transport
327 feedbacks and thus more likely to be captured using a more comprehensive chemistry scheme.
328 Furthermore, both simulations feature small changes in the troposphere. Overall, therefore, the
329 LINOZ scheme captures the gross characteristics of the ozone abrupt 4xCO₂ response expected
330 from previous studies. Note that most of this ozone response occurs in both simulations within the
331 5-20 years that comprise the “fast” response timescale, as shown in Chiodo et al. (2018) (see their
332 Figure 7b), although full equilibration at high latitudes does take somewhat longer (not shown).

333 In response to the ozone changes to 4xCO₂ both the OMA simulation and LINOZ ensemble
334 produce cooling in the tropical lower stratosphere and warming over high latitudes (Fig. 4c,d). The
335 amplitude of the cooling is ~1.5-2K in the tropical lower stratosphere, and is more-or-less collocated
336 with the region of largest ozone decreases. Further analysis of the temperature tendencies reveals



317 FIG. 4. Top: Colors show the annual averaged change in ozone number density in response to $4xCO_2$. Bottom:
 318 Colors show the annual averaged change in temperature in response to $4xCO_2$, relative to the $4xCO_2$ change in
 319 the NINT simulations. Results for OMA (left) and LINOZ (right) are shown in both rows and averaged over years
 320 5-20. One simulation is shown for OMA and the four-member ensemble mean response is shown for LINOZ.
 321 Black dashed contours in the bottom panels show climatological mean preindustrial control temperatures (contour
 322 interval: 10 C). Stippled regions are statistically significant and the black thick line shows the climatological
 323 mean tropopause in the preindustrial control NINT simulation.

337 that in our model the cooler temperatures in the tropics and subtropics ($40^\circ S-40^\circ N$) are associated
 338 with reduced radiative heating, primarily in the shortwave component (not shown). Dynamically,
 339 comparisons of the $4xCO_2$ changes in the residual mean stream function show a weaker response
 340 in LINOZ, relative to NINT (not shown). This ozone feedback on the Brewer-Dobson circulation,
 341 first identified in DallaSanta et al. (2021a), contributes to reduced upwelling, adiabatic cooling,
 342 and ozone transport within the lower tropical stratosphere. These circulation changes are therefore
 343 not the primary drivers of the temperature response; rather, they are primarily determined by the
 344 shortwave radiative response to ozone changes (CP2019).

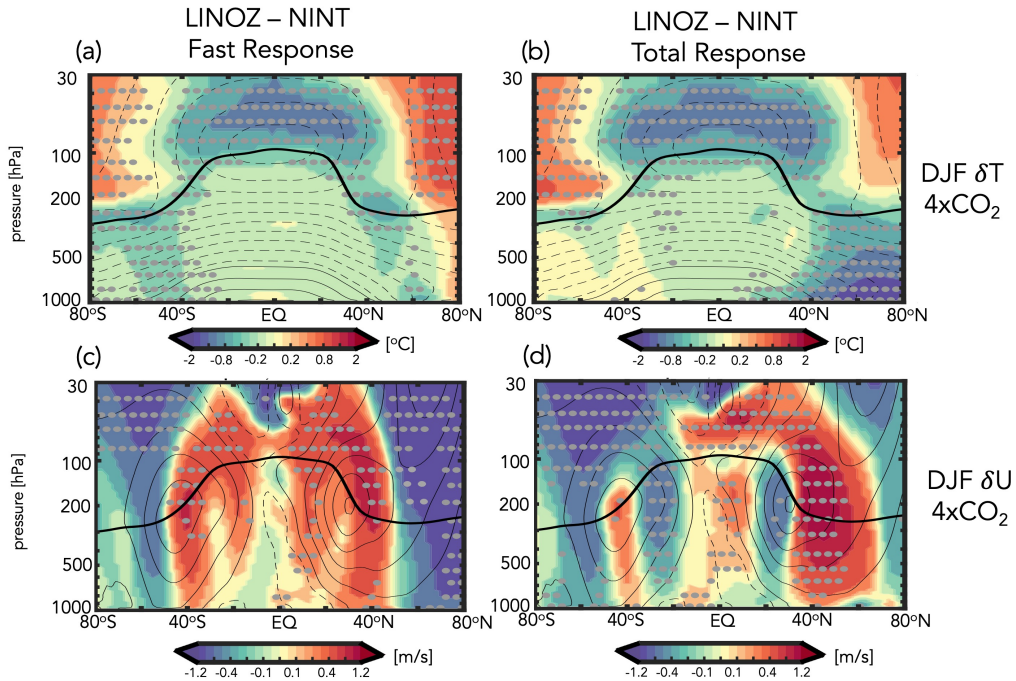
345 The temperature responses in both the OMA (Fig. 4c) and LINOZ (Fig. 4d) experiments are on
 346 the lower end of the 2-4K range documented in CP2019 as the differences shown reflect the 5-20

347 (not 100-150) year response (note that all colorbars used are consistent with that study to facilitate
348 comparisons with their results). An important point to note is that the temperature changes due to
349 ozone are of a similar magnitude to the temperature changes due to $4xCO_2$ alone in the tropical
350 lower stratosphere (i.e., considering no ozone feedback), where the stratosphere cools by $\sim 2K$ in
351 the NINT ensemble (not shown). The ozone changes present in LINOZ (and OMA) therefore
352 represent a substantial (same order of magnitude) feedback on the CO_2 -induced cooling in the
353 stratosphere at this altitude.

354 *c. Ozone Feedback on Northern Hemisphere Midlatitude Jet: Fast Response*

355 The temperature response due to ozone is dynamically consequential for the troposphere to the
356 extent that it modifies temperature gradients (and winds) in the lower stratosphere. Indeed, the
357 LINOZ ensemble shows a strong reduction of lower stratospheric temperature gradients in both
358 hemispheres on both the fast and total response timescales (Fig. 5a,b). In the fast response, this
359 reduction in the meridional temperature gradient near the tropopause has important consequences
360 for the midlatitude jet in both hemispheres, particularly in the NH where it strengthens above and
361 along the jet core and weakens on the poleward flank of the jet over latitudes north of $\sim 50^\circ N$ (Fig.
362 5c). The winds also accelerate equatorward of the jet core, relative to NINT, in both hemispheres,
363 although the response is only statistically significant in our model in the NH. This ozone-induced
364 response in the jet is very similar to the pattern of the wind response reported in CP2019 (see their
365 Figures 4 and 5). As with the temperature changes occurring in the lower stratosphere, the wind
366 response to ozone changes is similar in magnitude to the $4xCO_2$ response (Fig. 1), again suggesting
367 a substantial modulation of the circulation in both hemispheres by ozone changes alone.

374 In the lower troposphere (850 hPa) the fast response evident in the zonal mean zonal winds
375 (Fig. 5c) is characterized by weakened winds north of $60^\circ N$ over nearly all longitudes (Fig. 6a).
376 By comparison, the weakened wind response south of $60^\circ N$ is far more zonally asymmetric and
377 concentrated over the Atlantic ocean, where negative wind anomalies are flanked equatorward by
378 positive wind anomalies (Fig. 6a). Time series of the zonal winds over the North Atlantic at 850
379 hPa show evidence of this anomalous weakening of the jet in LINOZ occurring during the first
380 20 years (Fig. A3a), despite large internal variability. A similar response is also evident at 300
381 hPa (not shown), suggesting that the anomalous equatorward shift over the Atlantic during the fast

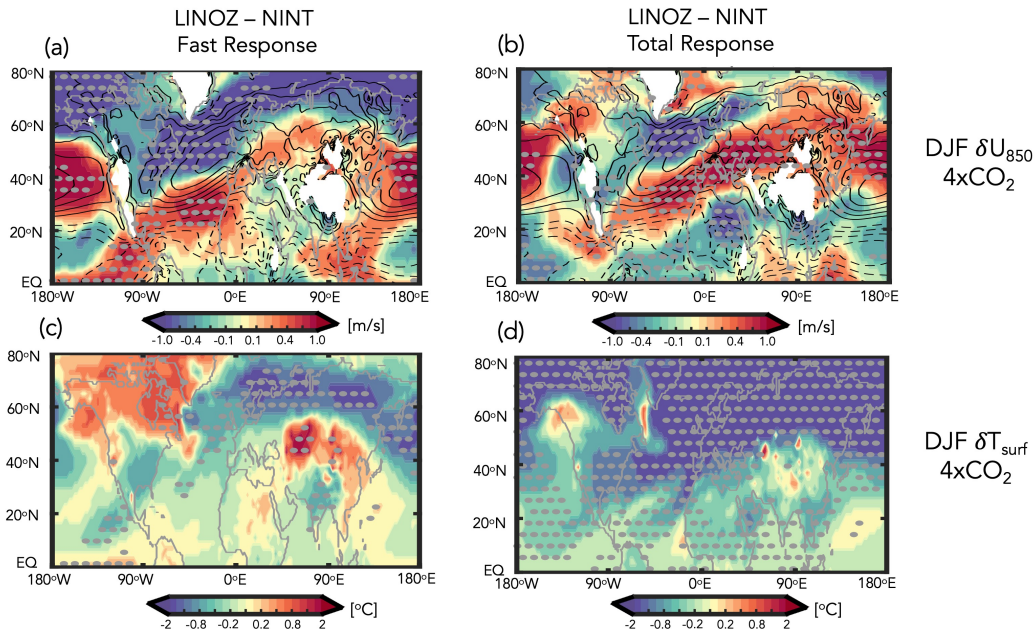


368 FIG. 5. Colors show the LINOZ-NINT ensemble mean difference in the DJF response of the zonal mean
 369 temperatures, T (top) and zonal winds, U (bottom) in response to an abrupt quadrupling of CO_2 . Both LINOZ
 370 and NINT ensembles consist of four members. Responses are decomposed into “fast” (a,c) and “total” (b,d)
 371 changes. Contours denote climatological mean DJF values (T contour interval: 10 C; U contour interval: 8 m/s).
 372 Stippled regions are statistically significant and the black thick line shows the climatological mean tropopause in
 373 the preindustrial control simulation.

382 response comprises a barotropic response that extends from the upper troposphere down into the
 383 lower troposphere.

384 The LINOZ-NINT wind dipole at 850 hPa over the North Atlantic is very similar to the fast
 385 wind response captured in the fully interactive OMA simulation (Fig. 3c). This consistency with
 386 the response in OMA is also reflected at 300 hPa, where in both LINOZ and OMA configurations
 387 the winds accelerate between the climatological subtropical and midlatitude eddy-driven jets (Fig.
 388 A2a,c).

389 Over the Pacific, by comparison, the OMA and LINOZ responses are different, consistent with
 390 CP2019, who also found no robust ozone feedback over that basin (see their Figure 5). This lack
 391 of a robust ozone feedback over the Pacific is generally consistent with previous modeling and
 392 observational studies showing a much stronger signal of “downward” stratosphere-troposphere



402 FIG. 6. Same as Figure 5, except showing the LINOZ-NINT DJF response in the 850 hPa zonal winds, U_{850}
 403 (top) and surface temperatures, T_{surf} (bottom). Contours in top panels denote climatological mean DJF values
 404 of U_{850} (contour interval: 2 m/s). Note the similarity between the “fast” wind response shown in (a) and the
 405 CP2019 results (their Figure 6).

393 coupling over the Atlantic, relative to the Pacific (see Baldwin et al. (2021) and references therein),
 394 although this difference between sectors remains speculative and warrants closer inspection beyond
 395 the scope of the present study.

396 In addition to the near surface wind changes, the weakening of the North Atlantic jet in the
 397 LINOZ simulations is associated with warming over northern North America and cooling over the
 398 North Atlantic and over Eurasia, resembling the negative phase of the NAO (Fig. 6c). A similar
 399 surface temperature anomaly was identified in CP2019 (see their Figure 7) and in our model occur
 400 in conjunction with positive sea level pressure (SLP) anomalies over the Arctic (Appendix Figure
 401 A4, left), both features being reminiscent of a negative NAO.

406 *d. Ozone Feedback on Northern Hemisphere Midlatitude Jet: Total Response*

407 Interestingly, while the fast responses in the winds and temperatures in the LINOZ ensemble
 408 are highly consistent with the results from CP2019, our model also simulates a distinct “total”

409 response characterized by strong cooling over the Arctic from the surface to the mid-to-upper
410 troposphere (Fig. 5b). This cooling, which was not identified in CP2019, results in enhanced
411 mid-to-lower tropospheric temperature gradients, prompting a strong acceleration of the winds at
412 50°N exceeding 2 m/s (Fig. 5d). Note that this acceleration at 50°N does not occur during the fast
413 response, during which the winds weaken poleward of 50°N (Fig. 5c).

414 Zonally, the cooling over the Arctic occurring in the LINOZ ensemble during the total response
415 primarily reflects hemispheric-wide cooling over the Arctic associated with an expansion of the
416 North Atlantic Warming Hole (Fig. 6d, see also Zhang et al. (2023)). Thus, while both fast and
417 total responses feature a similar weakening of the winds over the North Atlantic, this enhancement
418 of meridional temperature gradients in the lower and mid troposphere drives an eastward extension
419 and acceleration of the Atlantic jet over Europe and a poleward shift over the Pacific ocean during
420 the total response (Fig. 6b). Time series of the zonal winds at 850 hPa show this strengthening
421 of the midlatitude jet in LINOZ occurring on longer timescales (Fig. A3b), particularly over the
422 Pacific and, to a lesser extent, over Europe. The jet acceleration over Europe is, by comparison,
423 more pronounced in the upper troposphere (not shown) (Bellomo et al. 2021; Orbe et al. 2023).

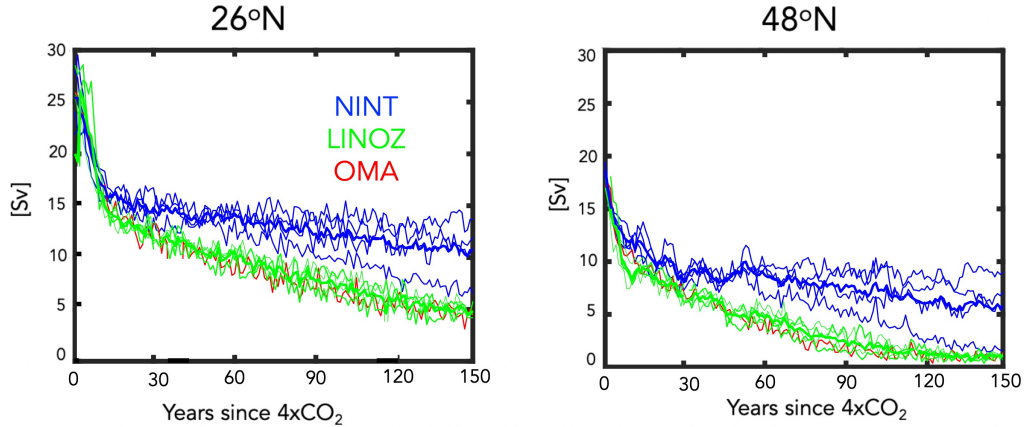
424 By comparison, the eastward extension of the Atlantic jet is not evident during the fast response,
425 nor is the poleward shift over the Pacific. This distinct behavior of the jet over the Pacific and
426 Europe during the total response was also not captured in CP2019 and, as such, comprises a
427 coupled ozone-ocean feedback that is distinct from what was reported in that study.

428 *e. Total Ozone Feedback: Modulation by the AMOC*

429 The “total” responses in the tropospheric winds and temperatures that occur in the LINOZ
430 ensemble are not obviously linked to ozone-driven temperature changes in the stratosphere, which
431 do not extend into the troposphere. What, then, is the driver of the lower tropospheric high latitude
432 cooling, if it is not directly linked to ozone-driven stratospheric temperature changes?

433 As expected from the OMA and NINT results presented in Zhang et al. (2023) and summarized
434 in Figure 2, we find that the strong cooling that occurs over the NH in the total LINOZ response is
435 also related to a weakening of the AMOC at 4xCO₂ (Mitevski et al. (2021); Orbe et al. (2023)). In
436 particular, Figure 7 shows stronger weakening of the AMOC in the LINOZ (green lines) ensemble,
437 relative to NINT (blue lines) at both 26°N (left) and at 48°N (right). Despite large internal

Annual Mean $4xCO_2$ AMOC Response



443 FIG. 7. Evolution of the annual mean maximum overturning stream function below 900 m in the Atlantic ocean,
444 evaluated at 26°N (left) and 48°N (right) in response to $4xCO_2$. Results for the LINOZ and NINT ensembles are
445 shown in green and blue, respectively (thick lines denote ensemble means). Red lines show the response in the
446 OMA simulation.

438 variability, the LINOZ ensemble mean shows a more rapid decline of the AMOC, a difference that
439 is evident at both latitudes. While the differences between the LINOZ and NINT ensemble means
440 are most pronounced following year 20, a difference of $\sim 2\text{-}3$ SV is already established by year 20.
441 **Furthermore, results from a Welch's t-test show that the differences between the LINOZ and NINT**
442 **ensembles become statistically significant at 48°N starting at year 8.**

447 Interestingly, comparisons of the AMOC behavior in LINOZ with the fully interactive OMA
448 simulation (red line) shows a striking similarity (and the mechanism of these changes is also
449 similar, as shown in Section 3f). This similarity is surprising, given that other (non-ozone) trace
450 gases and aerosols are also evolving in the OMA experiment. In particular, Rind et al. (2018),
451 using a previous version of the model, observed an indirect effect of natural aerosols (primarily
452 sea salt) on AMOC stability. They showed that aerosols enhanced the local cooling of SSTs
453 in regions of increased cloud cover in a warmer climate by acting as condensation nuclei and
454 thereby raising cloud optical thickness and ocean surface cooling. This surface cooling was then
455 linked to reduced evaporation relative to precipitation, resulting in anomalously positive surface

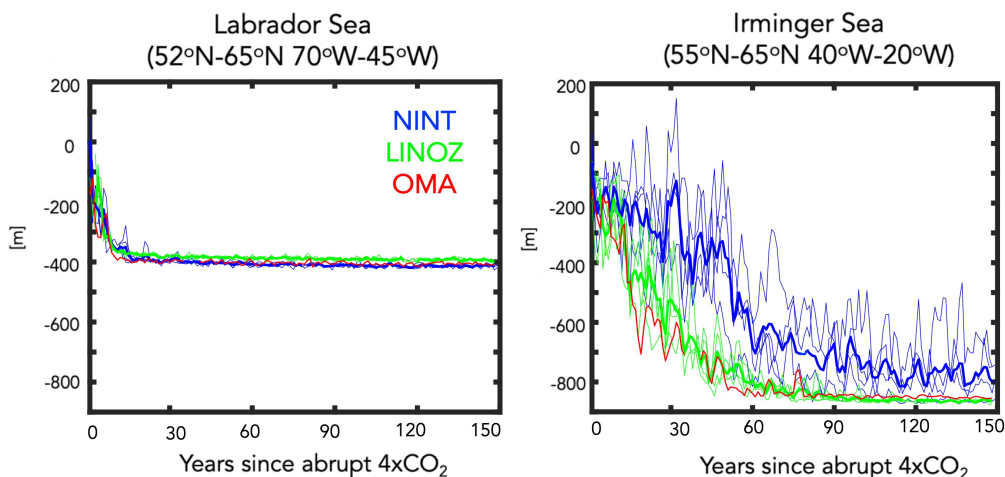
456 freshwater forcing and reduced North Atlantic Deep Water (NADW) production. That study,
457 however, focused on aerosol-induced AMOC cessations occurring on multicentennial timescales
458 long after the initial (abrupt) warming. By comparison, the results in Figure 7 identify an impact
459 of ozone on the ensemble mean AMOC responses that occurs within the first 20 years of the
460 initial CO₂ forcing – that is, over the period during which ozone is also rapidly evolving (Chiodo
461 et al. 2018) and stratospheric temperature gradients are most impacted by changes in ozone (not
462 aerosols). Our results, therefore, highlight that during this time frame the AMOC can be as (if not
463 more) sensitive to wind-driven buoyancy changes forced by stratospheric ozone anomalies as they
464 are to aerosol-induced changes in freshwater forcing.

465 Before elucidating the mechanism of the AMOC changes in the LINOZ ensemble, we first
466 identify the region over which the largest differences in mixed layer depth begin to emerge between
467 the LINOZ (OMA) and NINT simulations. In particular, the weaker AMOC in the LINOZ and
468 OMA runs is found to be accompanied by a rapid reduction in mixed layer depths, which occur
469 primarily in the Irminger Sea region (55°N-65°N, 40°W-20°W) (Figure 8). Over that region, an
470 ensemble mean LINOZ vs. NINT difference of ~200 m is established by year ~20, **at which point**
471 **a Welch’s t-test confirms that the ensemble differences are statistically significant.** The mixed layer
472 depth differences among the configurations in the Labrador Sea are, by comparison, negligible.
473 East of the Irminger Sea (i.e., 55°N-65°N, 20°W-0°) we also identify differences between the
474 ensembles (not shown), but these emerge later, suggesting that the Irminger Sea changes are likely
475 the initiators of the differences in AMOC behavior between the NINT and LINOZ ensembles. The
476 same region was identified in Romanou et al. (2023) as being key for determining the sensitivity of
477 the AMOC in various SSP 2-4.5 ensemble runs, albeit for simulations conducted using the lower
478 vertical resolution GISS climate model.

483 *f. Ozone Feedback Dependence on the AMOC: Linking Fast and Total Responses*

484 Is the fact that the AMOC declines more rapidly in the LINOZ ensemble – and the OMA
485 simulation – a response to the ozone changes in those simulations or just a coincidence? In the fast
486 response the zonal wind changes over the North Atlantic reflect a weakening of the jet core that is
487 flanked equatorward by positive anomalies, resembling a negative NAO pattern. Indeed, a negative
488 (positive) NAO has been associated with a weaker (stronger) AMOC in idealized climate model

DJF 4xCO₂ Response in Mixed Layer Depth



479 FIG. 8. Changes in the DJF mixed layer depths, evaluated over the Labrador Sea (left) and Irminger Sea
 480 (right) in response to 4xCO₂, relative to the preindustrial control simulations. Results for the LINOZ and NINT
 481 ensembles are shown in green and blue, respectively (thick lines denote ensemble means). Red lines show the
 482 response in the OMA simulation.

489 experiments in which heat is artificially added (extracted) to/from the subpolar gyre, resulting in
 490 reduced (increased) NADW formation (Delworth and Zeng (2016)). Here we argue that such a
 491 mechanism is present in our model simulations, resulting in a long-term modulation of the NH
 492 midlatitude jet by ozone that occurs indirectly through changes in the AMOC.

493 In particular, Figure 9 shows maps of the surface zonal wind, surface friction speed, mixed layer
 494 depth, net heat fluxes, sea surface temperatures, and north-south heat and salinity ocean transports,
 495 averaged over years 1-5 (averages over years 5-20 are shown in Figure 10). In response to an abrupt
 496 quadrupling of CO₂, the surface winds weaken over the subpolar North Atlantic region in NINT,
 497 leading to a weak acceleration of the zonal winds on the poleward flank of the North Atlantic jet
 498 (~60°N-70°N) (Fig. 9a, top). Over the subpolar North Atlantic the weakening of the surface winds
 499 leads to a significant reduction in surface friction speed (Fig. 9b, top). At the same time, there
 500 is a reduction in mixed layer depths (Fig. 9c, top), as well as increased heat flux into the ocean
 501 (in the form of reduced latent heat fluxes out of the ocean) (Fig. 9d, top) and warmer sea surface

502 temperatures (Fig. 9e, top). The reduced surface density during the first 20 years associated with
503 these warmer temperatures lead to a rapid decrease in mixed layer depth by some 200 m (Figure
504 8) and the overturning circulation by $\sim 40\%$ (Figure 7) in NINT. At these early years the changes
505 in meridional heat and salinity transports over the Irminger Sea are relatively small (Fig. 9fg, top).

506 However, in response to the ozone changes captured in the LINOZ ensemble during years 1-5,
507 there is an even stronger reduction in the surface zonal winds and friction speed (Fig. 9 ab, bottom),
508 consistent with the negative NAO response evident in the 850 hPa zonal winds (Fig. 6a). The
509 surface friction changes align closely with the reduced mixed layer depths which extend well into
510 the Irminger Sea region and over latitudes further south of the subpolar gyre (Fig. 9c, bottom).

511 The reductions in mixed layer depth that occur over the Irminger Sea are likely driven by the
512 reductions in surface wind speed which increase (primarily latent) heat fluxes into the ocean (Fig.
513 9d, bottom), driving warmer sea surface temperatures in LINOZ, relative to NINT (Fig. 9e,
514 bottom). The sign of the response of the heat fluxes in the subpolar gyre region is consistent with
515 previous studies showing that a positive (negative) phase of the NAO implies reduced (enhanced)
516 atmosphere to ocean heat fluxes (Delworth et al. (2017)). Furthermore, the spatial pattern of
517 the heat flux response is very similar to the NAO heat flux composites that were prescribed in
518 Delworth and Zeng (2016) and inferred from observations in Ma et al. (2020) (see their Figure
519 6), who showed that there is much greater heat loss from the ocean over the subpolar region in
520 association with a jet strengthening.

521 At the same time, the changes in freshwater forcing (P-E) during this time period are negligible
522 such that the net buoyancy forcing comprising the sum of both net heat and freshwater fluxes ($\sim Q+F$)
523 is positive. This stabilizing buoyancy forcing from surface warming makes the mixed layer depths
524 shallower by suppressing convective mixing, shutting down NADW production (Alexander et al.
525 (2000); Kantha and Clayson (2000)). There is also an initial change in the north-south heat and
526 salt transports that is collocated with the dipole anomaly in the surface friction speed, promoting
527 anomalous poleward salt and heat transport into the subpolar gyre (Fig. 9fg, bottom). This feature
528 is confined to the top few ocean layers (not shown) and the implied anomalous heat transport could
529 be contributing to the warmer sea surface temperatures in that region, in addition to the surface
530 heat flux changes. Note that the emergence of these surface changes happens somewhat earlier
531 than the response in the AMOC, which shows clearer differences by year ~ 10 (Fig. 7). While a

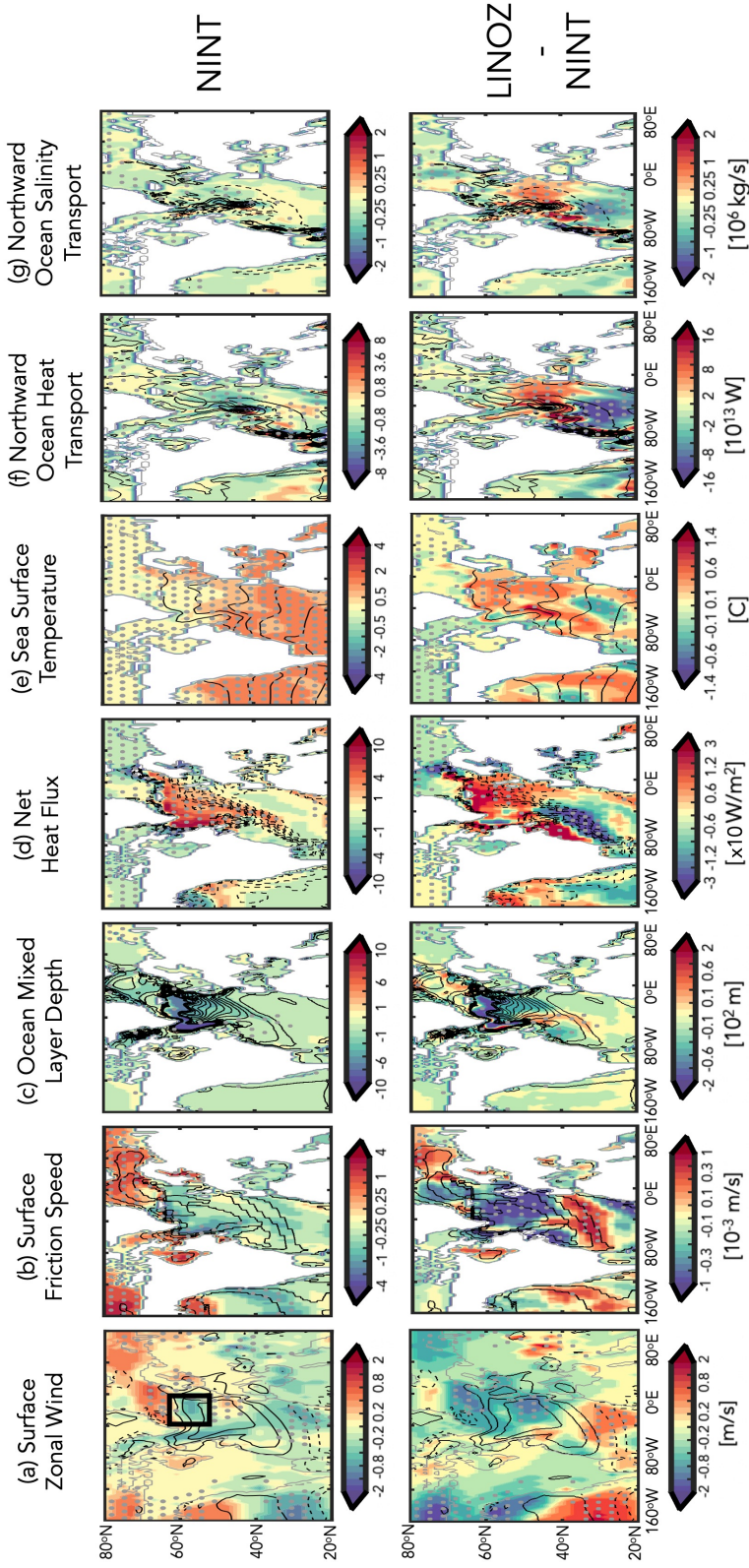
532 thorough examination of potential lags in the response of the AMOC, relative to the surface, are
533 beyond the scope of this study, this will be examined in future work.

542 Over the ensuing years (5-20) a similar pattern is maintained in the LINOZ ensemble (Figure
543 10, middle row). The reduction in NADW, however, results in reduced northward heat and salinity
544 transports (Fig. 10 fg, middle) throughout the ocean column. While this results in cooler SSTs
545 south of the subpolar gyre region (Fig. 10e, middle), which otherwise might enhance the density
546 of the near-surface water masses, the reduced northward salinity transports prevent the AMOC
547 from restarting. Interestingly, the results from the OMA simulation show a very similar response
548 as the LINOZ ensemble (Figure 10, bottom row), suggesting that stratospheric ozone changes in
549 that simulation are also likely the primary driver of the weaker AMOC in that model configuration.
550 This sequence of processes linking the surface wind changes to anomalous heat fluxes and reduced
551 NADW is basically identical to what is outlined in Figure 4 of Delworth and Zeng (2016) and
552 Figure 1 of Khatri et al. (2022). Additional analysis of the 2xCO₂ simulations, which feature a
553 stronger AMOC decline in OMA (and LINOZ) compared to NINT (Figure 2), reveals that a similar
554 mechanism for reduced NADW production occurs at lower CO₂ forcing (not shown).

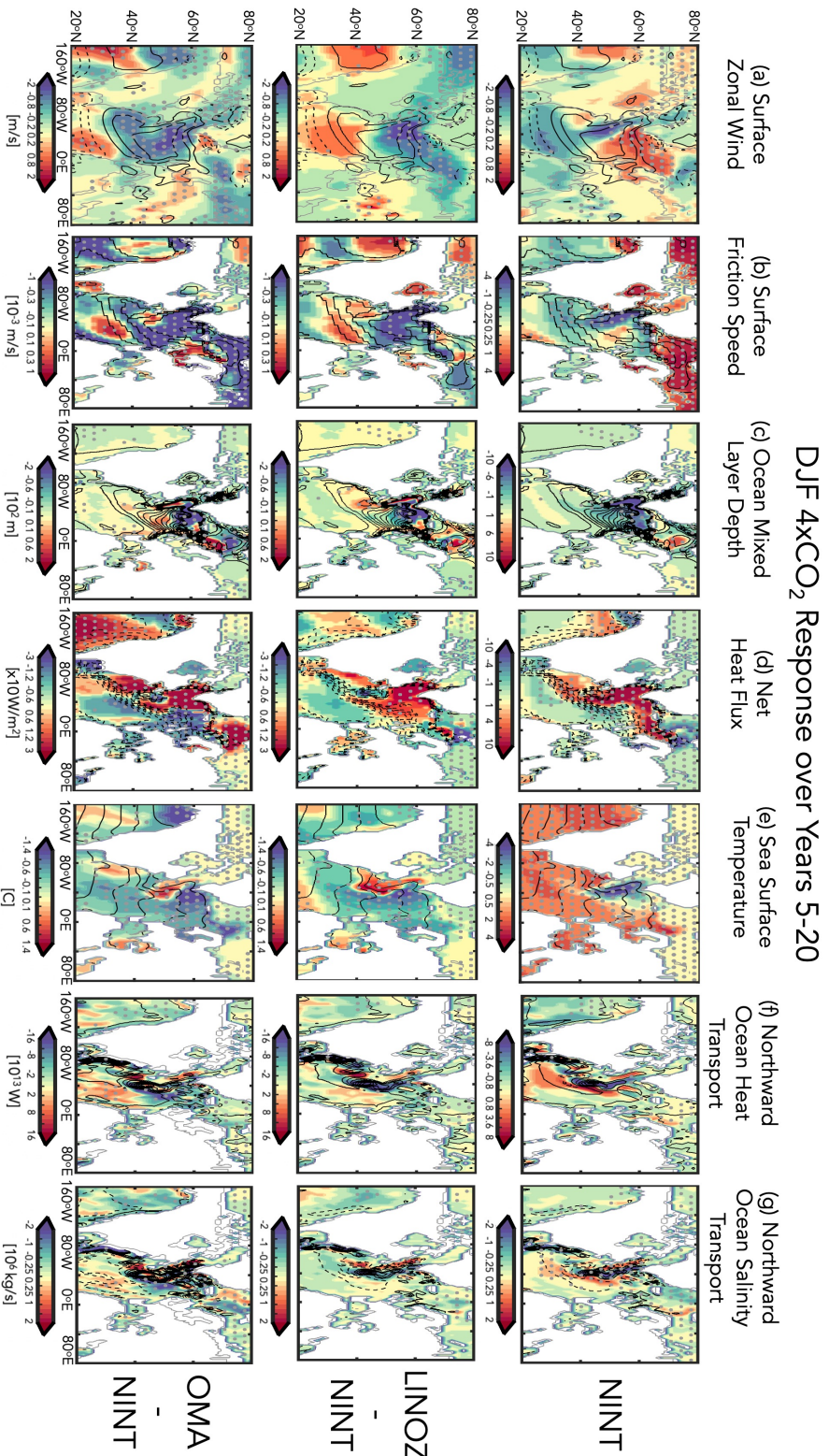
558 Examining the timescale of the responses of the variables shown in Figures 9 and 10 reinforces
559 the strong coupling between the changes in surface friction speed, sea surface temperature, latent
560 heat fluxes and mixed layer depth changes over the Irminger Sea region (Figure 11a-d). Despite
561 large internal variability, there is a clear separation between the LINOZ (and OMA) and NINT
562 ensembles that emerges ~ year 15 (black dashed lines). The changes in sensible heat emerge after
563 the latent heat fluxes (Fig. 11e), suggesting that the latter play a more important role in initializing
564 the heat flux differences in LINOZ (and OMA), relative to NINT.

566 Finally, while they may contribute to enhanced positive buoyancy forcing later in the integrations,
567 the freshwater forcing anomalies ($F = P - E$) are shown to be negligible during the initial years
568 following the abrupt quadrupling of CO₂ (Fig. 11f), indicating that the primary driver of the
569 initial difference between the LINOZ (and OMA) and NINT runs is related to the surface wind-
570 driven changes as they impact the latent heat fluxes into the ocean. This is consistent with Roach
571 et al. (2022) who showed a much stronger correlation between AMOC strength at 26°N and the
572 heat component of the surface buoyancy flux, relative to the freshwater component, in various
experiments using the Community Earth System Model version 1 (CESM1) in which the winds

DJF 4xCO₂ Response over Years 1-5

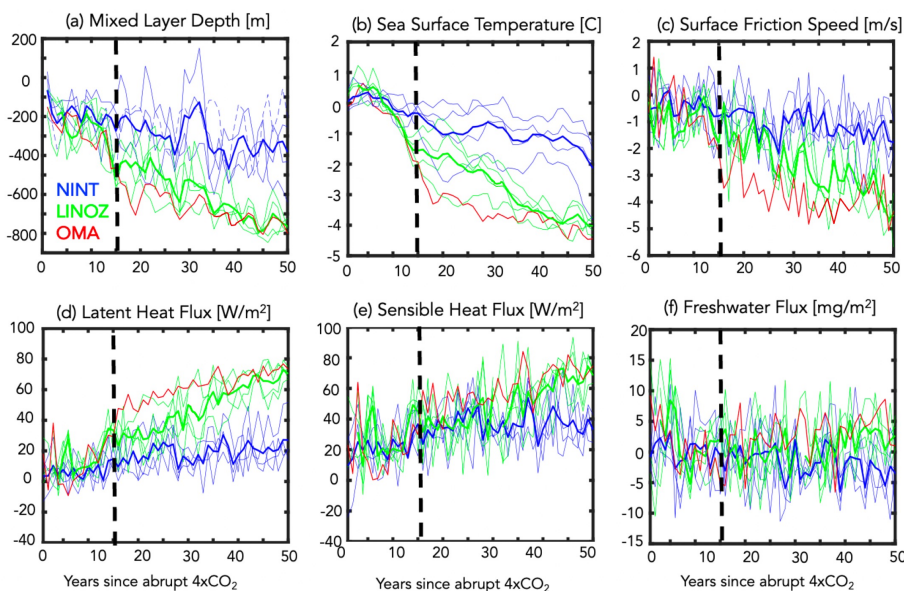


534 Fig. 9. Top panels: Colors show the December-January-February (DJF) response of the surface zonal wind (a), surface friction speed (b), ocean
 535 mixed layer depth (c), net heat flux (sum of sensible plus latent heat) (d), sea surface temperature (e) and northward heat (f) and salt (g) transports in
 536 response to an abrupt quadrupling of CO₂. Results are shown for the 4-member ensemble averaged NINT configuration. Bottom panels: Same as top
 537 panels, except showing the LINOZ minus NINT ensemble mean difference. For both top and bottom panels, responses have been averaged over years
 538 1-5 since “branching” from the preindustrial control simulation. Stippled regions are statistically significant and black contours denote climatological
 539 mean preindustrial control DJF values. Contour intervals: surface zonal wind [2 m/s], surface friction speed [2.5×10^{-3} m/s], mixed layer depth [60 m],
 540 net heat flux [30 W/m²], sea surface temperature interval [2°C], northward heat flux [2×10^{12} W], and northward salt flux [10^6 kg/s]. The black box in
 541 (a) bounds the Irminger Sea region over which the spatial averages in Figure 8b and Figure 11 are evaluated.



555 Fig. 10. Same as Figure 9, except showing the responses, averaged over years 5-20. An extra row at the bottom has been added, showing the OMA -
 556 NINT differences, where the ensemble members shown in Figures 1, 2 and 3 have been used. Same contour intervals and colorbars have been used as
 557 in Fig. 9.

DJF 4xCO₂ Response over Irminger Sea



577 FIG. 11. Changes in the DJF mixed layer depths (a), sea surface temperatures (b), surface friction speed (c),
 578 latent heat fluxes (d), sensible heat fluxes (e) and precipitation minus evaporation (f) in response to 4xCO₂,
 579 relative to the preindustrial control simulations. Averages are performed over the Irminger Sea (55°N-65°N,
 580 40°W-20°W) and the x-axis is restricted to years 1-50 in order to highlight the fast timescales on which the mixed
 581 layer depths, surface friction speed and heat fluxes evolve together. Results for the LINOZ and NINT ensembles
 582 are shown in green and blue, respectively (thick lines denote ensemble means). Red lines show the response
 583 in the OMA simulation. Black vertical lines indicate ~15 at which point the mixed layer depth responses in
 584 the LINOZ and NINT ensembles diverge. Note that the freshwater flux unit of 1 mg/m² per second (\equiv 0.0864
 585 mm/day \equiv 3.1 cm/year) is used, because at 5°C it contributes approximately the same ocean density flux as the
 586 heat flux unit of 1 W/m² (Large and Yeager (2009)).

573 over the subpolar gyre were nudged to reanalysis values. Note that in our model other potential
 574 contributors to freshwater forcing from sea ice do reveal differences between the LINOZ, OMA
 575 and NINT ensembles, but these emerge several years (i.e., years ~20-30) after the changes in sea
 576 surface temperatures and heat fluxes (not shown).

587 *g. Ozone Driver of AMOC Changes: Fixed SST and SIC Results*

588 So far, we have shown that the stratospheric ozone changes that occur in response to $4\times\text{CO}_2$
589 result in a negative NAO response over the North Atlantic (Fig. 5,6). In our model this triggers a
590 more rapid decline of the AMOC (Fig. 7) through surface-wind driven changes in heat fluxes into
591 the ocean (Fig. 9,10). While the time series analysis (Fig. 11) reveals that the AMOC changes
592 in the LINOZ (OMA) ensemble occur on similar timescales as the wind (and heat flux) changes,
593 one potentially confounding factor is the fact that the AMOC reduction itself results in reduced
594 wind speeds over the subpolar gyre region. These reduced near-surface winds are associated with
595 an anomalous anticyclonic flow pattern (Fig. A4, left; also discussed in Gervais et al. (2019);
596 Romanou et al. (2023); Orbe et al. (2023)), which could contribute to the reduced heat fluxes and
597 subsequent changes in NADW production. Therefore, to more convincingly link the surface wind
598 speed changes to the stratospheric ozone changes aloft, we next examine results from the fixed
599 preindustrial control SST and SIC experiments.

600 Figure 12 shows the ozone-induced zonal wind and temperature changes averaged over the last
601 twenty years of the fixed preindustrial control SST and SIC experiments in which the time-varying
602 zonally varying ozone from the $4\times\text{CO}_2$ LINOZ ensemble is prescribed (Fig. 12 a,b). Recall that in
603 the fixed SST and SIC experiments, only the ozone evolution differs from the preindustrial control
604 simulation, as CO_2 , SSTs and SIC are all set to preindustrial values. Comparisons with results
605 from the fully coupled LINOZ “fast” response (see Fig. 5a,c) reveal a very similar picture. This
606 similarity between the fully coupled fast response and the fixed preindustrial control SST and SIC
607 experiments is striking, both featuring a similar change in the NH jet associated with reduced
608 temperature gradients in the lower stratosphere as first reported in CP2019.

609 Comparisons of the 850 hPa zonal winds and surface temperatures over the North Atlantic (Fig.
610 12c,d) also reveal a strikingly similar response between the fully coupled ensemble and the fixed
611 preindustrial control SST and SIC experiments (compare with Fig. 6a,c). Over the Atlantic this
612 similarity also holds in the sea level pressure response (Fig. A4, right). The consistency in the
613 sea level pressure changes is interesting as it suggests that over the North Atlantic stratospheric
614 ozone changes alone can result in a significant reduction in the near surface winds that is on the
615 same order (if not larger than) the $4\times\text{CO}_2$ response. In our coupled atmosphere-ocean model

616 this additionally results in heat flux changes that are large enough to reduce NADW production,
617 resulting in a significant (i.e. $\sim 30\text{-}40\%$) long-term change in AMOC strength.

618 Finally, though not reported in depth here, we have performed an additional four-member en-
619 semble that is identical to the fixed SST and SIC runs, with respect to external forcings (i.e.,
620 preindustrial background CO_2 , LINOZ $4\times\text{CO}_2$ O_3), except run using the coupled atmosphere-
621 ocean model. Preliminary analysis of the “fast response” (5-20 years) in these experiments (not
622 shown) reveals very consistent ozone feedbacks on stratospheric temperatures, zonal mean winds
623 and 850 hPa zonal winds, compared to those captured in the coupled LINOZ $4\times\text{CO}_2$ simulations.
624 Over longer timescales (> 30 years), however, the response of the coupled ocean-atmosphere sys-
625 tem is more muted in the absence of any background $4\times\text{CO}_2$ forcing, especially the responses in
626 surface winds, net heat fluxes into the ocean and mixed layer depths. This result is perhaps not
627 surprising, given that the reduced surface zonal winds and mixed layer depths over the subpolar
628 gyre were identified as responses to an AMOC weakening in the ocean model employed in this
629 study (Orbe et al. 2023). This suggests that the AMOC response to stratospheric ozone feedbacks
630 depends sensitively on the background CO_2 forcing, although a systematic examination of this
631 dependence is beyond the scope of the current manuscript and will be explored in future work.

640 4. Conclusions

641 Here we have used the NASA GISS coupled atmosphere-ocean high-top model (E2.2-G) to
642 examine how coupled changes in stratospheric ozone and the ocean circulation both influence the
643 abrupt $4\times\text{CO}_2$ response of the NH midlatitude jet. Our key results are as follows:

- 644 • The NH midlatitude jet response to $4\times\text{CO}_2$ is modulated by coupled feedbacks from both
645 stratospheric ozone and the AMOC, which occur on “fast” (5-20 year) and “total” (100-150
646 year) timescales, respectively.
- 647 • In the “fast” response, the zonal mean jet weakens (strengthens) on its poleward (equatorward)
648 flank, consistent with reduced LS temperature gradients associated with ozone loss in the
649 tropics. This response is zonally asymmetric and is expressed as a negative NAO-like pattern,
650 consisting of weaker zonal surface winds over the North Atlantic, as reported in CP2019.

LINOZ – NINT Fixed SST Changes

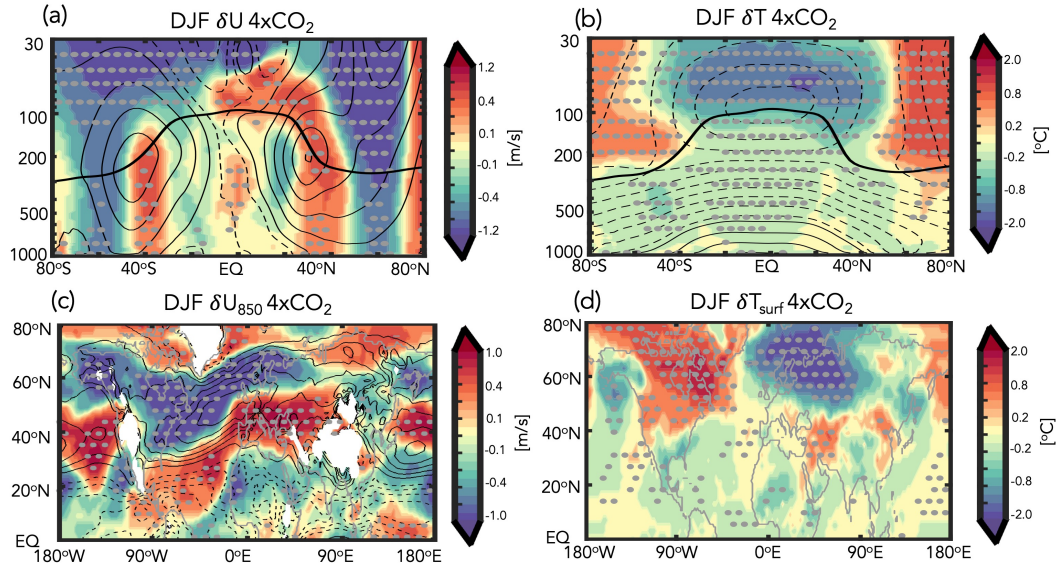


FIG. 12. Top panels: Colors show the $4xCO_2$ ensemble mean response in zonal mean zonal winds, U (a), temperatures, T (b), 850 hPa zonal winds, U_{850} (c) and surface temperature, T_{surf} (d) in the prescribed SST and SIC experiments in which the time-evolving $4xCO_2$ ensemble mean LINOZ ozone response is prescribed. Note that SSTs, SICs and background CO_2 are all set to preindustrial values. Averages are shown over the last 20 years (years 40-60) of the integrations. Black contours, where shown, denote climatological mean preindustrial control DJF values (U contour interval: 8 m/s; T contour interval: 10 C; U_{850} contour interval: 2 m/s). Stippled regions are statistically significant and the black thick line in the top panels shows the climatological mean tropopause in the preindustrial control simulation.

- The weaker winds over the North Atlantic occurring during the “fast” response are associated with increased (primarily latent) heat fluxes into the ocean, which initially result in warmer SSTs over the subpolar gyre region, reducing NADW production and leading to more rapid weakening of the AMOC.
- A reduced AMOC leads to widespread cooling over the Arctic which enhance mid-to-lower tropospheric temperature gradients, resulting in an eastward acceleration of the Atlantic jet and a poleward shift of the Pacific jet. The regional pattern of this “total” response is consistent with previously reported impacts of a weakened AMOC on the NH midlatitude jet (e.g., Bellomo et al. (2021); Liu et al. (2020); Orbe et al. (2023); Zhang et al. (2023)).

660 Taken together, the findings listed above indicate that the stratospheric ozone feedback on the NH
661 midlatitude jet reported in CP2019 is coupled to the behavior of the AMOC during the “fast”
662 response, wherein the jet weakens over the North Atlantic. In our model, this wind response
663 extends to the surface, resulting in reduced heat fluxes out of the subpolar gyre region and a more
664 rapid decline of the AMOC. On longer timescales, these changes in the AMOC subsequently
665 drive a poleward shift in the NH midlatitude jet. Unlike the “fast” response, this “total” timescale
666 response in the NH jet to changes in stratospheric ozone has not been previously reported, to the
667 best of our knowledge. This may reflect differing sensitivities of the AMOC among models and
668 our results will, of course, need to be tested using other models to assess robustness.

669 Another intriguing result from this study is that the stronger decline of the AMOC in the LINOZ
670 ensemble does not appear to be a coincidence. Rather, in our model, the “fast” ozone and “total”
671 AMOC feedbacks on the NH jet are coupled through surface-wind driven changes in heat fluxes
672 into the ocean. Key here is the fact that this sensitivity in the AMOC is driven only by changes in
673 stratospheric ozone, which we have isolated from changes in other trace gases and aerosols.

674 This last point is important to note, as previous studies have long shown that interactive atmo-
675 spheric composition can strongly influence the AMOC, but place an almost exclusive focus on the
676 role of aerosols (Booth et al. (2012); Cowan and Cai (2013); Swingedouw et al. (2015); Zhang et al.
677 (2013, 2019); Robson et al. (2022)). In particular, Rind et al. (2018) identified a larger sensitivity
678 of the AMOC response to global warming using an interactive configuration of the CMIP5 version
679 of the GISS climate model (GISS-E2-R), compared to a non-interactive version. In that study, mul-
680 ticentennial cessations of the AMOC were found to occur in simulations in which natural aerosols
681 (primarily sea salt) were allowed to locally cool sea surface temperatures through their influence
682 on cloud optical thickness; these cooler SSTs were then linked to reduced evaporation relative
683 to precipitation, resulting in positive surface freshwater forcing and reduced NADW production.
684 Unlike in that study, the mechanism proposed here only invokes changes in stratospheric ozone,
685 not aerosols, and to the best of our knowledge, no study has previously demonstrated an impact of
686 stratospheric ozone changes alone on the AMOC response to a quadrupling of CO₂. Despite the
687 different mechanisms at play, however, our results are generally consistent with those from Rind
688 et al. (2018) in that they highlight the need for renewed focus on surface flux observations to help
689 assess overturning stability.

690 An important caveat with our results is related to known biases in vertical mixing and NADW
691 production in the ocean component of the GISS model (Miller et al. (2021); Romanou et al.
692 (2023)) which likely explain why the low-top version of the coupled atmosphere-ocean climate
693 model (E2.1-G) exhibits a more sensitive AMOC response to a quadrupling of CO₂, compared
694 to some other models (Bellomo et al. (2021)). An important point to highlight, however, is that
695 the high-top model employed in this study is much less sensitive, as the AMOC weakens by ~10
696 SV in response to 4xCO₂, compared to a complete collapse in E2.1-G (see Figure 31 in Rind
697 et al. (2020)). That study showed that this may be related to differences in the parameterization of
698 rainfall evaporation associated with moist convective precipitation, which they show has a strong
699 influence on the AMOC sensitivity in the GISS model via its effect on moisture loading in the
700 atmosphere. While an exhaustive comparison between the models is beyond the scope of this
701 study, the relevant point here is that the 4xCO₂ AMOC response simulated in the E2.2-G NINT
702 ensemble is well within the CMIP5 and CMIP6 ranges documented in Mitevski et al. (2021) (see
703 their Supplementary Figure S3).

704 An important next step for future research is to identify the forcings under which this influence
705 from stratospheric ozone is evident. Our preliminary analysis of the coupled atmosphere-ocean
706 response to 4xCO₂ stratospheric ozone changes reveals a much more muted ocean response in
707 experiments where the background CO₂ forcing is fixed to preindustrial values, compared to
708 simulations in which CO₂ increases. This suggests that the ozone feedback on the AMOC depends
709 on the background CO₂ forcing and may hinge on the model's so-called "hysteresis" or threshold
710 beyond which the AMOC continues to weaken, even upon reversal of the forcing. Indeed, recent
711 studies (Romanou et al. 2023; Orbe et al. 2023) have identified hysteresis not only in the ocean model
712 employed in this study, but also in the much broader CMIP6 model archive (Jackson et al. 2022).
713 This hypothesis, however, remains highly speculative and future work will focus on exploring the
714 CO₂ forcing-dependence of the ozone feedback and its relationship with hysteresis.

715 Another related issue concerns the need to examine whether the ozone feedback occurs in
716 more comprehensive scenarios using transient forcing. Although not examined in equal depth,
717 results from the more realistic 1%CO₂ transient simulations also show a greater weakening of the
718 AMOC in OMA, relative to NINT, indicating that the findings presented here are not an artifact
719 of the abruptness of the forcing (not shown). Analysis of the more comprehensive historical and

720 future Shared Socioeconomic Pathway (SSP) (Meinshausen et al. (2020)) integrations is currently
721 underway to identify other factors, including aerosols and the solar cycle (Muthers et al. (2016)),
722 which are likely to influence the ocean circulation. For sake of brevity, however, we reserve further
723 discussion of the more comprehensive results for future work.

724 Finally, our results linking the fast timescale jet response to the ensuing AMOC changes un-
725 derscore the profound impact that changes in lower stratospheric winds alone can have on surface
726 climate, as highlighted in Sigmond and Scinocca (2010). Quite remarkably, our fixed SST and SIC
727 experiments showed that these lower stratospheric wind changes are driven primarily by changes
728 in ozone and not by background changes in CO₂ or in sea surface boundary conditions. Taken
729 together, our results suggest that more attention needs to be paid to understanding the time-evolving
730 response of the coupled Earth system to future ozone changes, with a focus on changes in ocean
731 heat transport and how these feed back on the NH jet stream.

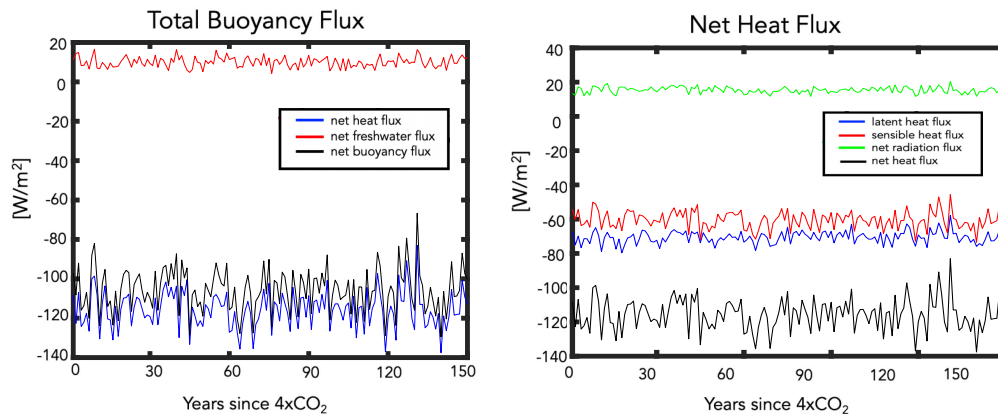
732 *Acknowledgments.* C.O. acknowledges helpful discussions with Lettie Roach, Ivan Mitevski
733 and Lorenzo Polvani. G.C. acknowledges support by the SNSF with the “Ambizione” grant
734 N. PZ00P2_180043. Climate modeling at GISS is supported by the NASA Modeling, Analysis and
735 Prediction program, and resources supporting this work were provided by the NASA High-End
736 Computing (HEC) Program through the NASA Center for Climate Simulation (NCCS) at Goddard
737 Space Flight Center.

738 *Data availability statement.* The NINT and OMA GISS E2.2-G simulations used in the study
739 are available at the CMIP6 archive via the Earth System Grid Federation ([https://esgf-node.
740 llnl.gov/](https://esgf-node.llnl.gov/)), where NINT and OMA are respectively denoted as “physics version 1” and “physics
741 version 3”. The specific simulations used here are the PiControl, abrupt-2xCO₂, and abrupt-
742 4xCO₂ r1i1p1f1 (NINT) and r1i1p3f1 (OMA) runs. Output needed to reproduce all figures
743 showing the additional three NINT 4xCO₂ simulations, fixed SST simulations as well the four-
744 member LINOZ ensemble is available online at [https://gmao.gsfc.nasa.gov/gmaoftp/
745 corbe/AMOC_Linoz/Data/](https://gmao.gsfc.nasa.gov/gmaoftp/corbe/AMOC_Linoz/Data/). All GISS ModelE components are open source and available at
746 <http://www.giss.nasa.gov/tools/modelE/>.

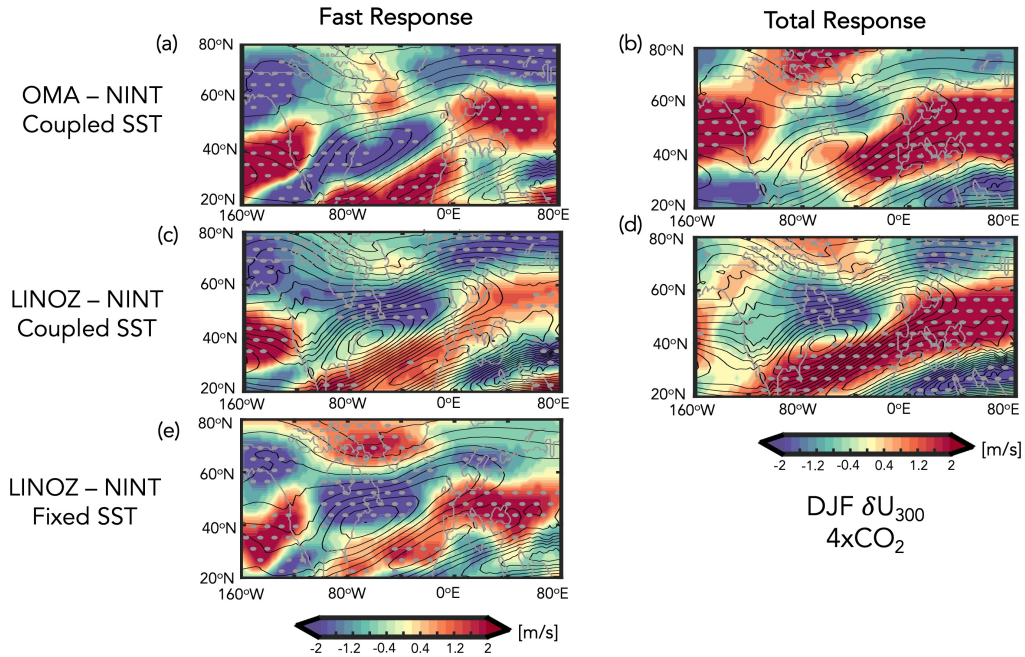
747

APPENDIX

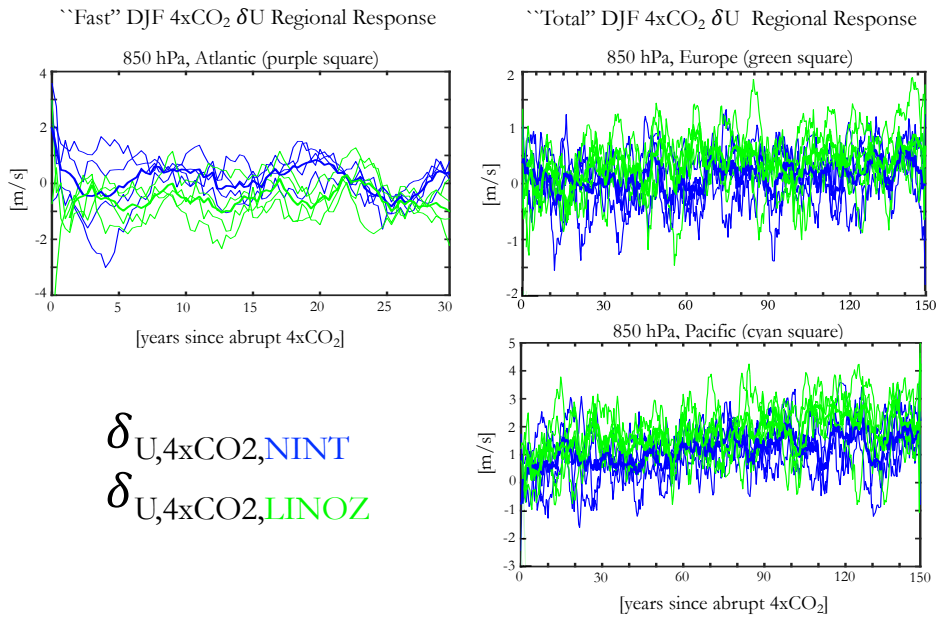
Annual Mean PiControl Climatological
Flux Decompositions over the Irminger Sea



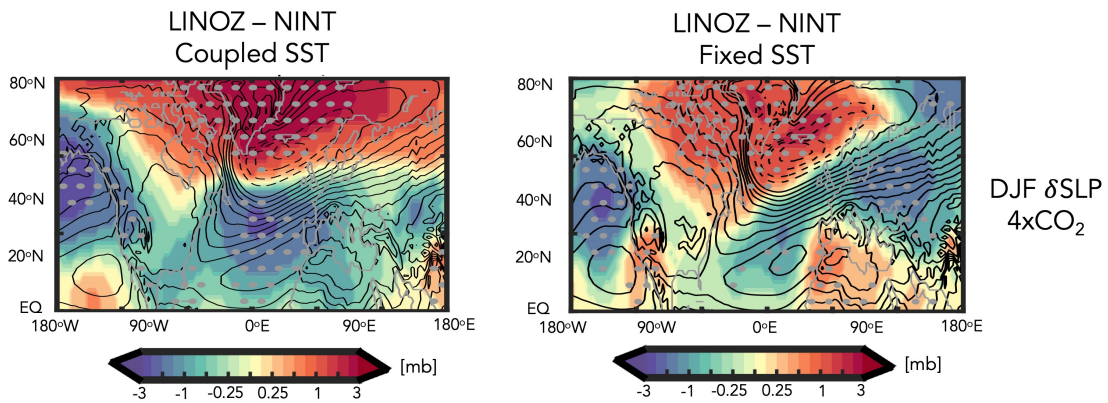
748 FIG. A1. Left: Decomposition of the net surface buoyancy flux (black) into contributions from net heat
749 (blue) and net freshwater (red) fluxes. Right: Further decomposition of the net surface heat flux (black) into
750 contributions from latent heat fluxes (Q_E (blue)), sensible heat fluxes (Q_H (red)), and combined solar and
751 longwave radiative fluxes (Q_S+Q_L (green)). Results are shown for 150 years of the NINT preindustrial control
752 (PiControl) simulation, evaluated over the Irminger Sea.



753 FIG. A2. Colors show the coupled atmosphere-ocean OMA - NINT (a,b) and LINOZ - NINT (c,d) $4xCO_2$
 754 changes in the DJF 300 hPa zonal winds. One ensemble member is used in the top panels, compared to four
 755 members in the middle row. Panel e shows results from the atmosphere-only ensemble in which the time-evolving
 756 $4xCO_2$ ensemble mean LINOZ ozone response is prescribed and the SSTs, SICs, and background CO_2 are set to
 757 preindustrial values. Left and right panels in the top and middle rows show the responses decomposed into “fast”
 758 (i.e. years 5-20) (a,c) and “total” (i.e. years 100-150) (b,d) responses. Averages over years 40-60 are shown
 759 for the prescribed SST and SIC experiments in panel e, which equilibrate much more rapidly, compared to the
 760 coupled experiments. Black contours denote climatological mean preindustrial control DJF values (U contour
 761 interval: 2 m/s) and stippled regions are statistically significant.



762 FIG. A3. Changes in the DJF zonal winds at 850 hPa, focusing on the “fast” (a) and “total” (b) responses to
 763 4xCO₂, relative to the preindustrial control simulations. The fast response is evaluated over the North Atlantic
 764 (50°W-10°W, 45°N-65°N). The slow response is evaluated over Europe (0°E-80°E, 45°N-65°N) and over the
 765 Pacific (150°E-150°W, 45°N-65°N). Results for the LINOZ and NINT ensembles are shown in green and blue,
 766 respectively (thick lines denote ensemble means).



767 FIG. A4. Left panel: Colors show the LINOZ minus NINT ensemble mean difference in the December-
 768 January-February (DJF) “fast” response of the sea level pressure to an abrupt quadrupling of CO_2 . Results are
 769 shown for the fully coupled atmosphere-ocean simulations. Right panel: The ensemble mean response in sea
 770 level pressure in the experiments in which the time-evolving $4\times\text{CO}_2$ ensemble mean LINOZ ozone response
 771 is prescribed and the SSTs, SICs, and background CO_2 are set to preindustrial values. Black contours denote
 772 climatological mean preindustrial control DJF values (contour interval: 10 mb). Stippled regions are statistically
 773 significant.

774 **References**

- 775 Alexander, M. A., J. D. Scott, and C. Deser, 2000: Processes that influence sea surface temperature
776 and ocean mixed layer depth variability in a coupled model. *Journal of Geophysical Research:
777 Oceans*, **105 (C7)**, 16 823–16 842.
- 778 Ayarzagüena, B., and Coauthors, 2020: Uncertainty in the response of sudden stratospheric
779 warmings and stratosphere-troposphere coupling to quadrupled CO₂ concentrations in CMIP6
780 models. *Journal of Geophysical Research: Atmospheres*, **125 (6)**, e2019JD032 345.
- 781 Baldwin, M. P., and Coauthors, 2021: Sudden stratospheric warmings. *Reviews of Geophysics*,
782 **59 (1)**, e2020RG000 708.
- 783 Barnes, E. A., and L. Polvani, 2013: Response of the midlatitude jets, and of their variability, to
784 increased greenhouse gases in the cmip5 models. *Journal of Climate*, **26 (18)**, 7117–7135.
- 785 Bauer, S. E., and Coauthors, 2020: Historical (1850–2014) aerosol evolution and role on climate
786 forcing using the GISS ModelE2. 1 contribution to CMIP6. *Journal of Advances in Modeling
787 Earth Systems*, **12 (8)**, e2019MS001 978.
- 788 Bellomo, K., M. Angeloni, S. Corti, and J. von Hardenberg, 2021: Future climate change shaped
789 by inter-model differences in Atlantic meridional overturning circulation response. *Nature Com-
790 munications*, **12 (1)**, 1–10.
- 791 Bellomo, K., V. L. Meccia, R. D’Agostino, F. Fabiano, S. M. Larson, J. von Hardenberg, and
792 S. Corti, 2023: Impacts of a weakened amoc on precipitation over the euro-atlantic region in the
793 ec-earth3 climate model. *Climate Dynamics*, 1–20.
- 794 Booth, B. B., N. J. Dunstone, P. R. Halloran, T. Andrews, and N. Bellouin, 2012: Aerosols
795 implicated as a prime driver of twentieth-century North Atlantic climate variability. *Nature*,
796 **484 (7393)**, 228–232.
- 797 Butler, A. H., D. W. Thompson, and R. Heikes, 2010: The steady-state atmospheric circulation
798 response to climate change–like thermal forcings in a simple general circulation model. *Journal
799 of Climate*, **23 (13)**, 3474–3496.

800 Ceppi, P., and D. L. Hartmann, 2015: Connections between clouds, radiation, and midlatitude
801 dynamics: A review. *Current Climate Change Reports*, **1 (2)**, 94–102.

802 Ceppi, P., G. Zappa, T. G. Shepherd, and J. M. Gregory, 2018: Fast and slow components of
803 the extratropical atmospheric circulation response to CO₂ forcing. *Journal of Climate*, **31 (3)**,
804 1091–1105.

805 Chiodo, G., and L. M. Polvani, 2019: The response of the ozone layer to quadrupled CO₂
806 concentrations: Implications for climate. *Journal of Climate*, **32 (22)**, 7629–7642.

807 Chiodo, G., L. M. Polvani, D. R. Marsh, A. Stenke, W. Ball, E. Rozanov, S. Muthers, and
808 K. Tsigaridis, 2018: The response of the ozone layer to quadrupled CO₂ concentrations. *Journal*
809 *of Climate*, **31 (10)**, 3893–3907.

810 Cowan, T., and W. Cai, 2013: The response of the large-scale ocean circulation to 20th century
811 Asian and non-Asian aerosols. *Geophysical Research Letters*, **40 (11)**, 2761–2767.

812 DallaSanta, K., C. Orbe, D. Rind, L. Nazarenko, and J. Jonas, 2021a: Dynamical and trace gas
813 responses of the quasi-biennial oscillation to increased CO₂. *Journal of Geophysical Research:*
814 *Atmospheres*, **126 (6)**, e2020JD034 151.

815 DallaSanta, K., C. Orbe, D. Rind, L. Nazarenko, and J. Jonas, 2021b: Response of the quasi-
816 biennial oscillation to historical volcanic eruptions. *Geophysical Research Letters*, **48 (20)**,
817 e2021GL095 412.

818 Delworth, T. L., and K. W. Dixon, 2000: Implications of the recent trend in the Arctic/North
819 Atlantic oscillation for the North Atlantic thermohaline circulation. *Journal of Climate*, **13 (21)**,
820 3721–3727.

821 Delworth, T. L., and F. Zeng, 2016: The impact of the North Atlantic oscillation on climate
822 through its influence on the Atlantic meridional overturning circulation. *Journal of Climate*,
823 **29 (3)**, 941–962.

824 Delworth, T. L., F. Zeng, L. Zhang, R. Zhang, G. A. Vecchi, and X. Yang, 2017: The central role
825 of ocean dynamics in connecting the North Atlantic oscillation to the extratropical component
826 of the Atlantic multidecadal oscillation. *Journal of Climate*, **30 (10)**, 3789–3805.

827 Eyring, V., S. Bony, G. A. Meehl, C. A. Senior, B. Stevens, R. J. Stouffer, and K. E. Taylor, 2016:
828 Overview of the Coupled Model Intercomparison Project Phase 6 (CMIP6) experimental design
829 and organization. *Geoscientific Model Development*, **9** (5), 1937–1958.

830 Garcia, R. R., and W. J. Randel, 2008: Acceleration of the Brewer–Dobson circulation due to
831 increases in greenhouse gases. *Journal of the Atmospheric Sciences*, **65** (8), 2731–2739.

832 Gervais, M., J. Shaman, and Y. Kushnir, 2019: Impacts of the North Atlantic warming hole in
833 future climate projections: Mean atmospheric circulation and the North Atlantic jet. *Journal of*
834 *Climate*, **32** (10), 2673–2689.

835 Grise, K. M., and L. M. Polvani, 2014: The response of midlatitude jets to increased CO₂:
836 Distinguishing the roles of sea surface temperature and direct radiative forcing. *Geophysical*
837 *Research Letters*, **41** (19), 6863–6871.

838 Grise, K. M., and L. M. Polvani, 2016: Is climate sensitivity related to dynamical sensitivity?
839 *Journal of Geophysical Research: Atmospheres*, **121** (10), 5159–5176.

840 Isaksen, I. S., and Coauthors, 2009: Atmospheric composition change: Climate–chemistry inter-
841 actions. *Atmospheric Environment*, **43** (33), 5138–5192.

842 Jackson, L., R. Kahana, T. Graham, M. Ringer, T. Woollings, J. Mecking, and R. Wood, 2015:
843 Global and european climate impacts of a slowdown of the amoc in a high resolution gcm.
844 *Climate dynamics*, **45**, 3299–3316.

845 Jackson, L. C., and Coauthors, 2022: Understanding amoc stability: the north atlantic hosing
846 model intercomparison project. *Geoscientific Model Development Discussions*, **2022**, 1–32.

847 Kantha, L. H., and C. A. Clayson, 2000: *Small scale processes in geophysical fluid flows*. Elsevier.

848 Kelley, M., and Coauthors, 2020: GISS-E2. 1: Configurations and climatology. *Journal of Ad-*
849 *vances in Modeling Earth Systems*, **12** (8), e2019MS002 025.

850 Khatri, H., R. G. Williams, T. Woollings, and D. M. Smith, 2022: Fast and slow subpolar ocean
851 responses to the North Atlantic oscillation: Thermal and dynamical changes. *Geophysical*
852 *Research Letters*, **49** (24), e2022GL101 480.

- 853 Li, F., and P. A. Newman, 2022: Prescribing stratospheric chemistry overestimates southern hemi-
854 sphere climate change during austral spring in response to quadrupled CO₂. *Climate Dynamics*,
855 1–18.
- 856 Lindzen, R. S., 1987: On the development of the theory of the QBO. *Bulletin of the American*
857 *Meteorological Society*, 329–337.
- 858 Liu, W., A. V. Fedorov, S.-P. Xie, and S. Hu, 2020: Climate impacts of a weakened Atlantic
859 meridional overturning circulation in a warming climate. *Science Advances*, **6 (26)**, eaaz4876.
- 860 Ma, L., T. Woollings, R. G. Williams, D. Smith, and N. Dunstone, 2020: How does the winter
861 jet stream affect surface temperature, heat flux, and sea ice in the North Atlantic? *Journal of*
862 *Climate*, **33 (9)**, 3711–3730.
- 863 Marshall, J., H. Johnson, and J. Goodman, 2001: A study of the interaction of the North Atlantic
864 oscillation with ocean circulation. *Journal of Climate*, **14 (7)**, 1399–1421.
- 865 McLinden, C., S. Olsen, B. Hannegan, O. Wild, M. Prather, and J. Sundet, 2000: Stratospheric
866 ozone in 3-D models: A simple chemistry and the cross-tropopause flux. *Journal of Geophysical*
867 *Research: Atmospheres*, **105 (D11)**, 14 653–14 665.
- 868 Meinshausen, M., and Coauthors, 2020: The shared socio-economic pathway (SSP) greenhouse
869 gas concentrations and their extensions to 2500. *Geoscientific Model Development*, **13 (8)**,
870 3571–3605.
- 871 Menzel, M. E., D. Waugh, and K. Grise, 2019: Disconnect between hadley cell and subtropical jet
872 variability and response to increased co2. *Geophysical Research Letters*, **46 (12)**, 7045–7053.
- 873 Meraner, K., S. Rast, and H. Schmidt, 2020: How useful is a linear ozone parameteriza-
874 tion for global climate modeling? *Journal of Advances in Modeling Earth Systems*, **12 (4)**,
875 e2019MS002 003.
- 876 Miller, R. L., and Coauthors, 2021: Cmp6 historical simulations (1850–2014) with GISS-E2. 1.
877 *Journal of Advances in Modeling Earth Systems*, **13 (1)**, e2019MS002 034.

878 Mitevski, I., C. Orbe, R. Chemke, L. Nazarenko, and L. M. Polvani, 2021: Non-monotonic
879 response of the climate system to abrupt CO₂ forcing. *Geophysical Research Letters*, **48** (6),
880 e2020GL090861.

881 Muthers, S., C. C. Raible, E. Rozanov, and T. F. Stocker, 2016: Response of the AMOC to reduced
882 solar radiation—the modulating role of atmospheric chemistry. *Earth System Dynamics*, **7** (4),
883 877–892.

884 Nowack, P. J., N. Luke Abraham, A. C. Maycock, P. Braesicke, J. M. Gregory, M. M. Joshi,
885 A. Osprey, and J. A. Pyle, 2015: A large ozone-circulation feedback and its implications for
886 global warming assessments. *Nature Climate Change*, **5** (1), 41–45.

887 O’Callaghan, A., M. Joshi, D. Stevens, and D. Mitchell, 2014: The effects of different sudden
888 stratospheric warming types on the ocean. *Geophysical Research Letters*, **41** (21), 7739–7745.

889 Orbe, C., and Coauthors, 2020: GISS Model E2.2: A climate model optimized for the middle
890 atmosphere—2. Validation of large-scale transport and evaluation of climate response. *Journal*
891 *of Geophysical Research: Atmospheres*, **125** (24), e2020JD033151.

892 Orbe, C., and Coauthors, 2023: Atmospheric response to a collapse of the north atlantic circulation
893 under a mid-range future climate scenario: A regime shift in northern hemisphere dynamics.
894 *Journal of Climate*, 1–52.

895 Reichler, T., J. Kim, E. Manzini, and J. Kröger, 2012: A stratospheric connection to Atlantic
896 climate variability. *Nature Geoscience*, **5** (11), 783–787.

897 Rind, D., J. Jonas, N. Balachandran, G. A. Schmidt, and J. Lean, 2014: The QBO in two GISS global
898 climate models: 1. Generation of the QBO. *Journal of Geophysical Research: Atmospheres*,
899 **119** (14), 8798–8824.

900 Rind, D., G. A. Schmidt, J. Jonas, R. Miller, L. Nazarenko, M. Kelley, and J. Romanski, 2018:
901 Multicentury instability of the Atlantic meridional circulation in rapid warming simulations with
902 GISS ModelE2. *Journal of Geophysical Research: Atmospheres*, **123** (12), 6331–6355.

903 Rind, D., R. Suozzo, N. Balachandran, A. Lacis, and G. Russell, 1988: The GISS global climate-
904 middle atmosphere model. Part I: Model structure and climatology. *Journal of the Atmospheric*
905 *Sciences*, **45** (3), 329–370.

906 Rind, D., and Coauthors, 2020: GISS Model E2.2: A climate model optimized for the mid-
907 dle atmosphere—model structure, climatology, variability, and climate sensitivity. *Journal of*
908 *Geophysical Research: Atmospheres*, **125** (10), e2019JD032 204.

909 Roach, L. A., E. Blanchard-Wrigglesworth, S. Ragen, W. Cheng, K. C. Armour, and C. M. Bitz,
910 2022: The impact of winds on AMOC in a fully-coupled climate model. *Geophysical Research*
911 *Letters*, e2022GL101203.

912 Robson, J., and Coauthors, 2022: The role of anthropogenic aerosol forcing in the 1850–1985
913 strengthening of the amoc in cmip6 historical simulations. *Journal of Climate*, **35** (20), 6843–
914 6863.

915 Romanou, A., and Coauthors, 2023: Stochastic bifurcation of the North Atlantic circulation under
916 a mid-range future climate scenario with the NASA-GISS ModelE. *Journal of Climate*.

917 Shaw, T., and Coauthors, 2016: Storm track processes and the opposing influences of climate
918 change. *Nature Geoscience*, **9** (9), 656–664.

919 Shaw, T. A., 2019: Mechanisms of future predicted changes in the zonal mean mid-latitude
920 circulation. *Current Climate Change Reports*, **5** (4), 345–357.

921 Shepherd, T. G., 2014: Atmospheric circulation as a source of uncertainty in climate change
922 projections. *Nature Geoscience*, **7** (10), 703–708.

923 Sigmond, M., and J. F. Scinocca, 2010: The influence of the basic state on the Northern Hemisphere
924 circulation response to climate change. *Journal of Climate*, **23** (6), 1434–1446.

925 Simpson, I. R., T. A. Shaw, and R. Seager, 2014: A diagnosis of the seasonally and longitudinally
926 varying midlatitude circulation response to global warming. *Journal of the Atmospheric Sciences*,
927 **71** (7), 2489–2515.

928 Smith, D. M., and Coauthors, 2019: The polar amplification model intercomparison project
929 (PAMIP) contribution to CMIP6: Investigating the causes and consequences of polar amplifica-
930 tion. *Geoscientific Model Development*, **12** (3), 1139–1164.

- 931 Swingedouw, D., P. Ortega, J. Mignot, E. Guilyardi, V. Masson-Delmotte, P. G. Butler, M. Khodri,
932 and R. S  ferian, 2015: Bidecadal North Atlantic ocean circulation variability controlled by
933 timing of volcanic eruptions. *Nature Communications*, **6 (1)**, 1–12.
- 934 Vallis, G. K., P. Zurita-Gotor, C. Cairns, and J. Kidston, 2015: Response of the large-scale structure
935 of the atmosphere to global warming. *Quarterly Journal of the Royal Meteorological Society*,
936 **141 (690)**, 1479–1501.
- 937 Visbeck, M., H. Cullen, G. Krahnmann, and N. Naik, 1998: An ocean model’s response to North
938 Atlantic oscillation-like wind forcing. *Geophysical Research Letters*, **25 (24)**, 4521–4524.
- 939 Voigt, A., and T. A. Shaw, 2015: Circulation response to warming shaped by radiative changes of
940 clouds and water vapour. *Nature Geoscience*, **8 (2)**, 102–106.
- 941 Yuval, J., and Y. Kaspi, 2020: Eddy activity response to global warming–like temperature changes.
942 *Journal of Climate*, **33 (4)**, 1381–1404.
- 943 Zhai, X., H. L. Johnson, and D. P. Marshall, 2014: A simple model of the response of the Atlantic
944 to the North Atlantic oscillation. *Journal of Climate*, **27 (11)**, 4052–4069.
- 945 Zhang, R., R. Sutton, G. Danabasoglu, Y.-O. Kwon, R. Marsh, S. G. Yeager, D. E. Amrhein, and
946 C. M. Little, 2019: A review of the role of the atlantic meridional overturning circulation in
947 atlantic multidecadal variability and associated climate impacts. *Reviews of Geophysics*, **57 (2)**,
948 316–375.
- 949 Zhang, R., and Coauthors, 2013: Have aerosols caused the observed atlantic multidecadal vari-
950 ability? *Journal of the Atmospheric Sciences*, **70 (4)**, 1135–1144.
- 951 Zhang, X., D. W. Waugh, and C. Orbe, 2023: Dependence of northern hemisphere tropospheric
952 transport on the midlatitude jet under abrupt co2 increase. *Journal of Geophysical Research:*
953 *Atmospheres*, e2022JD038454.